The University of Alberta
Printing Department
Edmonton, Alberta

THE UNIVERSITY OF ALBERTA

RELEASE FORM

NAME OF AUTHOR ..... YUSTO KAAHWA .....

TITLE OF THESIS ..... TUNNELING VIA PARTICLES .....

.....

.....

DEGREE FOR WHICH THESIS WAS PRESENTED MASTER OF SCIENCE..

YEAR THIS DEGREE GRANTED ..... 1973 .....

Permission is hereby granted to THE UNIVERSITY OF ALBERTA LIBRARY to reproduce single copies of this thesis and to lend or sell such copies for private, scholarly or scientific research purposes only.

The author reserves other publication rights, and neither the thesis nor extensive extracts from it may be printed or otherwise reproduced without the author's written permission.

THE UNIVERSITY OF ALBERTA

TUNNELING VIA PARTICLES

BY

© YUSTO KAAHWA

A THESIS

SUBMITTED TO THE FACULTY OF GRADUATE STUDIES AND RESEARCH

IN PARTIAL FULFILLMENT OF THE REQUIREMENTS FOR THE DEGREE

OF MASTER OF SCIENCE

DEPARTMENT OF PHYSICS

EDMONTON, ALBERTA

SPRING 1973

THE UNIVERSITY OF ALBERTA

FACULTY OF GRADUATE STUDIES AND RESEARCH

The undersigned certify that they have read, and recommend to the Faculty of Graduate Studies and Research for acceptance, a thesis entitled TUNNELING VIA PARTICLES by Yusto Kaahwa, in partial fulfillment of the requirements for the degree of Master of Science.

ABSTRACT

Giaever and Zeller (1968) have shown that small metallic particles in the barrier of a thin film tunnel junction cause a strong conductance dip to occur at zero bias in the tunneling characteristics. The characteristics are modified slightly if the particles are superconducting. These effects have been studied for Sn and Pb particles in the barrier of Al-I-Al tunnel junctions. The values of the transitions temperatures of Sn particles are found to be 4.15 ± 0.05°K and 4.05 ± .05°K for particles of average thicknesses 65 Å and 130 Å respectively. The difference between the values of the transition temperatures of Pb particles of average thicknesses 60 Å, 80 Å and 130 Å could not be distinguished. It was found to be 7.4 ±.05°K for all the three sets. The values of the energy gaps are found to be 2.59 mV, 2.65 mV, and 2.71 mV respectively at 1.08°K. The particle size distribution for a set of Pb particles was obtained from electron micrographs in order to test the Giaever-Zeller theory. Small effects due to the phonon spectrum of Pb particles were also observed.

ACKNOLWEDGEMENTS

I wish to express my gratitude to Dr. J.S. Rogers my research supervisor for suggesting this project and his continuous encouragement and guidance throughout the course of this work.

I am very grateful to Dr. M.A. Semary for many valuable discussions concerning this research and his assistance during some of the runs.

I wish to thank Messrs. J.C. Brunel and D. Cann for their help in observing the particles in the electron microscope. I wish to express my appreciation of the assistance offered by the technical staff and for supplying liquid nitrogen and liquid helium.

Finally I am very grateful to the Canadian Commonwealth Scholarship and Fellowship Administration and the Research Council of Canada for financial assistance.

TABLE OF CONTENTS

Chapter		Page
1	INTRODUCTION	1
2	MICROSCOPIC THEORIES OF SUPER-CONDUCTIVITY	3
	The BCS Theory	3
	(i) The Ground State and the Energy Gap	13
	(ii) Density of State	17
	(iii) Critical Temperature	18
	(iv) (a) The Critical Field	21
	(b) Size Effect on the Critical Field	23
3	MODELS OF TUNNELING	26
	A. Simple Model of Tunneling	26
	(a) Normal-Normal Case, I_{nn}	30
	(b) Normal-Superconducting Case, I_{ns}	30
	(c) Superconducting-Superconducting Case, I_{ss}	32
	B. Modified Model of Tunneling	33
	C. The Capacitor Model	35
4	EXPERIMENTAL PROCEDURES	47
	A. Sample Preparation	47
	I) Oxidation	48
	(i) Aluminium	48

Chapter		Page
4	(cont'd)	
	(ii) Tin	50
	(iii) Lead	50
	II) Particle Deposition	51
	B. Thickness Measurements	52
	C. Production of Low Temperature	56
	D. Conductance Measurements	58
5	EXPERIMENTAL RESULTS AND DISCUSSION	59
	A. Tin Particles	59
	(i) Sn-Sn^P-Sn Junctions	59
	(ii) Al-Sn^P-Al Junctions	63
	B. Lead Particles	71
	(i) Particle Distribution	71
	(ii) Al-Pb^P-Al Junctions	81
	(iii) Phonon Structure	87
6	CONCLUSION	93
	REFERENCES	94

LIST OF FIGURES

Figure		Page
2.1	A representation of the Fröhlich electron-electron interaction resulting from the exchange of a virtual phonon.	8
2.2	Two intersecting shells each of radius $k_F+\delta$ and thickness . The shaded area is a cross-section space phase available for scattering, with conservation of total momentum $\underline{K}$, of a pair of electrons with individual momenta restricted to the shell $k_F-\delta < k < k_F+\delta$.	11
2.3	Density of states in the BCS theory.	19
2.4	Temperature dependence of the energy gap in a superconductor.	22
2.5	Magnetization curve of a spherical superconductor.	24
3.1	Tunneling between two metals separated by a thin insulating layer.	27
3.2	Energy diagrams illustrating the density of states near the Fermi level, occupation of states and current-voltage characteristics in (a) normal-normal case (b) normal-superconducting case (c) superconducting-superconducting case.	31
3.3	Electron transfer process in (a) n-s with the particle going to state $\underline{k}'$ above $\underline{k}_F$ (b) n-s with the particle going to state $\underline{k}''$ below $\underline{k}_F$ (c) s-s with two possibilities of going to $\underline{k}'$ or $\underline{k}''$.	36
3.4	Particles embedded in oxide separating two metal films represented as two capacitors in series.	38

Figure		Page
3.5	(a) Particle excited levels (b) Voltage dependence of the conductance.	39
3.6	(a) The conductance of a set of particles with fixed capacitance C (b) The conductance of a number of particles f(C) with a distribution of capacitance C.	44
4.1	Sample preparation stages (a) Slightly oxidised M_1 film (b) M_3 particles on top of the oxide of M_1 (c) The surface of the particles lightly oxidised (d) Final film of M_2 counter electrode.	49
4.2	A quartz crystal thickness monitor (a) The oscillation of a single crystal; most of the mass displacement occurs at the crystal surface. (b) The circuit diagram of the crystal monitor used in this work. The integrated circuit is a Motorola MC 1024 P. (c) Crystal holder; very light springs are used to provide electrical contacts with the crystals.	53
4.3	The cryostat arrangement for the production of low temperature.	58
5.1	Voltage dependence of the conductance σ of three different junctions of Sn-Sn^P-Sn at 80°K.	60
5.2	Voltage dependence of the conductance σ of three different junctions of Sn-Sn^P-Sn at 4.2°K.	61
5.3	The conductance versus voltage for three different junctions of Sn-Sn^P-Sn at 2.1°K.	62

Figure		Page
5.4	Voltage dependence of the conductance σ of four different junctions of Al-Sn^P-Al at 80°K.	64
5.5	Voltage dependence of the conductance σ of different junctions of Al-Sn^P-Al at 4.2°K and the particle size dependence of $\sigma(0)$.	65
5.6	Conductance-voltage characteristics of five different junctions of Al-Sn^P-Al at 1.2°K.	66
5.7	Two-junctions in series-like behaviour for very thick particles.	68
5.8	The magnetic field effect on the conductance-voltage characteristic.	69
5.9	The temperature dependence of the conductance σ (a) average particle thickness, t = 65 Å (b) average particle thickness, t = 130 Å.	70
5.10	The temperature dependence of the normalized conductance σ_s/σ_n.	72
5.11	Particle distribution histogram for particles of thickness 60 Å.	78
5.12	Computer curve for $\sigma(V)$ versus voltage characteristic for Pb particles of average thickness 60 Å.	79
5.13	Measure (++ line) and calculated (solid line) conductance of a set of particles in the normal state, for particles of average thickness 60 Å.	80
5.14	The voltage dependence of the conductance of different junctions of Al-Pb^P-Al at 8.1°K.	82
5.15	Conductance versus voltage of four different junctions of Al-Pb^P-Al at 1.18°K.	83

Figure		Page
5.16	Second derivative of the conductance showing energy gaps for three different junctions.	85
5.17	(a) Conductance versus voltage with Pb particles normal (b) Multiple peaks of superconducting Al (c) Second derivative of curve (b).	86
5.18	The normalized conductance versus temperature for three different junctions of Al-Pb^{P}-Al.	88
5.19	Phonon structure for three different junctions of Al-Pb^{P}-Al. a'b', and c' are the second derivatives of a, b and c curves respectively.	90

LIST OF PLATES

Plate		Page
5.1	(a) Electron micrograph of lead particles of average thickness 180 Å (b) The diffraction pattern of particles in (a).	75
5.2	Electron micrographs of lead particles of average thickness (a) 60 Å (b) 130 Å.	76

CHAPTER 1

INTRODUCTION

Since Giaever's (1960) work on the experimental aspect of tunneling, there has been a sequence of measurements on both superconducting and normal metal-insulator-metal junctions. The results have continually puzzled both theoreticians and experimentalists leading them into one problem after another.

Minimum size for the occurrence of superconductivity has interested many workers. Anderson (1959) in his "Theory of Dirty Superconductors" predicted a lower size limit for the occurrence of superconductivity when the spacing of the electron energy levels is less than the energy gap. In his discussion of "Electrostatic Effect and Superconductivity in Tiny Particles" Markowitz (1967) modified the BCS Hamiltonian by adding on a Coulomb term and then minimised the ground state energy by considering, among other parameters, the sample size. These considerations led him to estimate the minimum size of a superconductor. Parmenter (1968) has derived an expression relating the dependence of the energy gap and transition temperature upon particle size. His calculations lead to rather too high values of critical size.

Zeller and Giaever (1968) have reported experimental results on small superconductors and proposed a capacitor model to account for the observed zero-bias resistance anomalies. They also observed particles as small as about 25 Å superconducting.

This thesis contains a report of the energy gaps and transition temperatures of small superconducting particles and some differences between direct tunneling and tunneling via particles in both normal and superconducting states. The size effect in superconductivity manifests itself in the energy gap and transition temperature which are different from those of a bulk material.

CHAPTER 2

MICROSCOPIC THEORIES OF SUPERCONDUCTIVITY

The BCS Theory

In the course of measurements of the decrease of electrical resistance of metals when they are cooled, Kamerlingh Onnes in 1911 found that mercury lost all of its resistance suddenly at about 4°K. Onnes called this state of no resistance the "superconducting state". For many years this phenomenon defied theoretical explanations. The first attempt was made by Gorter and Casimir (1934). They suggested a two-fluid model which stipulates that a fraction x of the metallic electrons remain normal at the transition temperature, T_c, while the remainder (1 - x) is condensed into the superconducting state. According to this model, the fraction x is given by

$$x = \left(\frac{T}{T_c}\right)^4 \quad , \qquad 2.1$$

the specific heat in the superconducting state is

$$C_{es} = 3\gamma \frac{T^3}{T_c^2} \qquad 2.2$$

where γ is the Sommerfeld constant, and the critical field is given by

$$H_c = H_o\left(1 - \frac{T^2}{T_c^2}\right) \quad . \qquad 2.3$$

These results were not in perfect agreement with experimental results.

The next step was made by London (1935) who derived "London equations" by introducing a characteristic constant λ_L called the penetration depth. But the Meissner effect required that a field already inside the material in the normal state should be expelled when the material becomes superconducting and this was not accounted for. London added another equation by postulating that

$$\dot{\underline{J}}_s = \frac{c}{4\pi\lambda_L^2}\,\underline{E} \quad , \qquad 2.4$$

$$\nabla\times\underline{J}_s = -\frac{c}{4\pi\lambda_L^2}\,\underline{H} \quad . \qquad 2.5$$

London's results together with those of Gorter and Casimir were used to fit experimental results but not successfully.

With the discovery of the isotope effect by Maxwell (1950) and Reynolds et al (1950) showing that lattice vibrations were involved in the superconducting state, a new approach was needed. Pippard (1953) introduced a non-local theory as a modification of the London theory, with a new parameter ξ called the coherence length. In terms of the microscopic theory, ξ may be considered as

the typical size of the "Cooper pairs". In the London equation

$$\underline{J}(\underline{r}) = - \frac{c}{4\pi\lambda_L^2} \underline{A}(\underline{r}) = - \frac{ne^2}{cm} \underline{A}(\underline{r}) \quad , \qquad 2.6$$

where

$$\lambda_L^2 = \frac{mc^2}{4\pi ne^2} \quad ,$$

Pippard introduced a dependence of the penetration depth on the electronic mean free path, L, such that

$$\underline{J}(\underline{r}) = - \frac{ne^2}{m} \frac{\xi(L)}{\xi_o} \underline{A}(\underline{r}) \quad , \qquad 2.7$$

where ξ_o is a constant of the superconductor in question. Derivation for the field penetration into a semi-infinite slab gives the field

$$H(x) = He\ e^{-x/\lambda} \qquad 2.8$$

where

$$\lambda = \lambda_L \sqrt{\frac{\xi_o}{\xi_L}} \quad .$$

Earlier on Pippard had shown that under low temperatures and high frequencies the mean free path may be longer than the skin depth, the electrons become less effective as current carriers and Ohm's law

$$\underline{J}(\underline{r}) = \sigma(L)\ \underline{E}(\underline{r}) \qquad 2.9$$

is no longer a reasonable approximation, but rather the current at a point must be determined by the total field over the distances of the order of the mean free path. Reuter and Sondheimer (1948) derived an expression for this anomalous skin effect of the form

$$\underline{J}(\underline{r}) = \frac{3\sigma}{4\pi L} \int \frac{\underline{r}(\underline{r}.\underline{E})}{r^4} e^{-r/L} \, d\tau \quad . \qquad 2.10$$

As analogous to equation (2.10), Pippard proposed a relation for the electromagnetic response of a superconductor of the form

$$J(r) = \frac{3ne^2}{4\pi\xi_o m} \int \frac{\underline{r}(\underline{r}.\underline{A}(\underline{r}))}{r^4} e^{-r/\xi} \, d\tau \quad . \qquad 2.11$$

A more successful explanation for the superconducting phenomenon has been presented by Bardeen, Cooper and Schrieffer (1957) known as the BCS theory. The BCS theory was set up to show that superconductivity was bound up with the behaviour of the conduction electrons; while the properties of the crystal lattice do not change, the crystal lattice plays an important part and that the superconducting-to-normal transition is a second order phase change.

Fröhlich (1950) had postulated that an electron-phonon interaction was able to couple two electrons such that they could behave as if it was an electron-electron

interaction. In this picture, an electron with momentum $\underline{k}_1$ interacts with the lattice emitting a phonon of momentum $\underline{q}$ and leaving the electron scattered with momentum $\underline{k}_1'$. The phonon is then absorbed by a second electron with momentum $\underline{k}_2$ which changes to momentum $\underline{k}_2'$ on absorption of the phonon, figure 2.1. By the law of conservation of momentum,

$$\underline{k}_1 = \underline{k}_1' + \underline{q}$$

$$\underline{k}_2' = \underline{k}_2 + \underline{q} = \underline{k}_2 + \underline{k}_1 - \underline{k}_1'$$

$$\underline{k}_1' + \underline{k}_2' = \underline{k}_1 + \underline{k}_2 \quad . \qquad 2.12$$

While the momentum and the energy are conserved between the initial and the final states, anything can happen in between the emission and the absorption of the phonon. If the life time, Δt, of this intermediate state is very short, there will be a large uncertainty in its energy ΔE according to the uncertainty principle

$$\Delta E . \Delta t \simeq h$$

in which case the energy need not be conserved in the emission and absorption process. Cooper (1956) carried forward this idea saying that there are correlations between electrons of opposite spin and these correlations are produced by the interaction between the electrons.

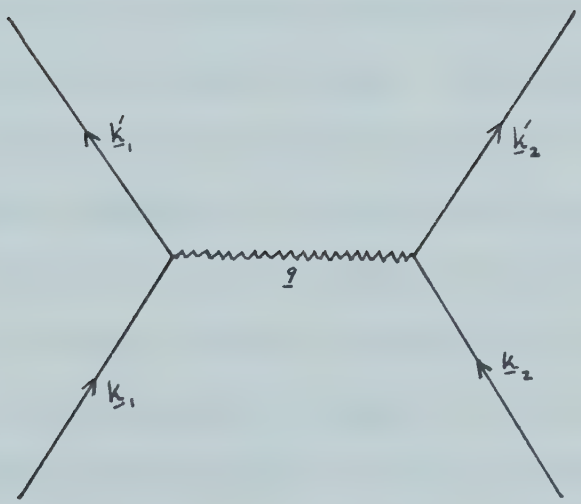

Figure 2.1

A representation of the Frohlich electron-electron interaction resulting from the exchange of a virtual phonon.

While in a classical model a very strong two-particle repulsion between two electrons implies that the two electrons would never get very close to one another, at very low temperatures the system can gain energy by going into a highly correlated state, Cooper (1959). Cooper postulated that the interaction producing the correlations is between electrons via the lattice.

When an electron collides with a lattice wave, it may be scattered producing some resistance. At $T = 0°K$, there are no lattice vibrations and the phonon part of the resistance goes to zero. But an electron can excite a virtual lattice wave which in turn interacts with another electron. Alternatively one can say that when an electron moves through a lattice of infinitely heavy lattice points, the lattice is polarized and another electron moving through it at a later time feels a distorted potential due to the polarization. The distorted potential is a function of position and time and shows up as a retarded interaction between two electrons.

As a two body correlation, the anti-parallel correlation function is assumed to be of the form

$$\rho_{\uparrow\downarrow} = \frac{1}{4} n^2 + f(\underline{r},\underline{K}) \quad , \qquad 2.13$$

where n is the density of electrons, $f(\underline{r},\underline{K})$ is the extra

correlation produced by the interaction between electrons, $\underline{r}$ is the relative coordinate of the two electrons involved and $\underline{K}$ is their total momentum.

For the ground state, single particle states are filled to the Fermi surface but the electron-electron interactions described above seem to be weak and varying slowly over the Fermi surface. In addition the energy involved in the normal-superconducting transition is very small. Cooper made a guess that the correlated states will involve single particle excitations in a small shell near the Fermi surface, figure 2.2. If we restrict ourselves to pair correlations, we shall want to know the interaction which takes a pair of electrons from one state to another state in this shell. The total momentum of the pair is conserved and the phase space available for transition from one state to another state of a given momentum is a strong function of the total momentum, $\underline{K}$, and is a maximum when $\underline{K} = 0$. It is found that the effective interaction between electrons of singlet spin is stronger than that of triplet spin due to the exchange terms in the electron-electron matrix element. If all the pair correlations have the same total momentum, the maximum correlation of the entire wave function can be obtained. For dynamical and statistical reasons there is a strong preference for momentum zero, singlet spin correlations

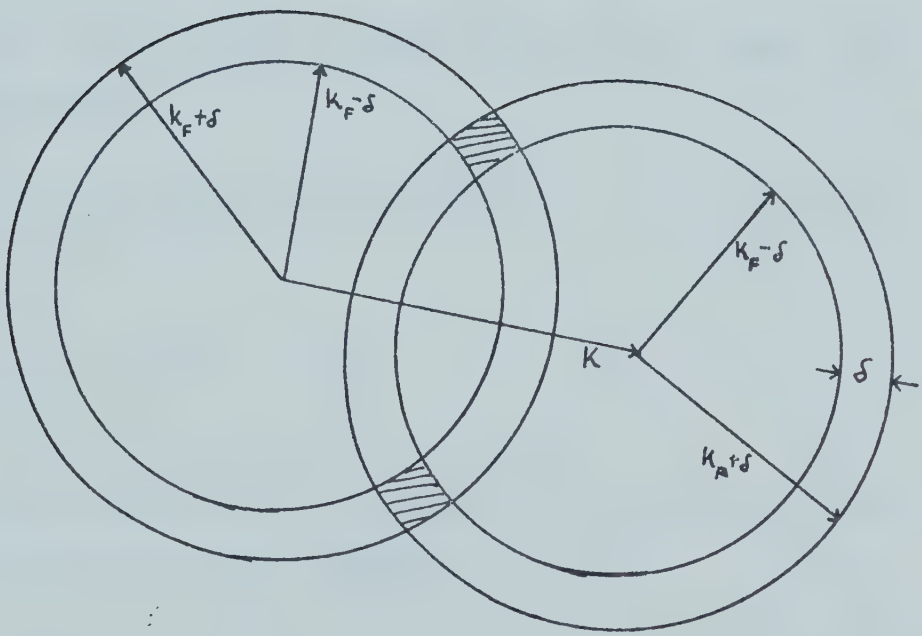

Figure 2.2. Two intersecting shells each of radius $k_F + \delta$ and thickness δ. The shaded area is a cross-section space phase available for scattering, with conservation of total momentum $\underline{K}$, of a pair of electrons with individual momenta restricted to the shell $k_F - \delta < k < k_F + \delta$.

and for statistical reasons alone there is a strong preference for all the correlations to have the same momentum. For these preferences the wave function Φ to represent electrons with the lowest possible potential energy is made up of wave functions of the form

$$\psi(\underline{P}\uparrow)\ \psi(-\underline{P}\downarrow) \qquad 2.14$$

where $\psi(\underline{P}\uparrow)$ describes an electron with momentum $\underline{P}$ and spin up and $\psi(-\underline{P}\downarrow)$ an electron with momentum $-\underline{P}$ and spin down. Φ is then represented as a total sum of these functions

$$\Phi(r_1,r_2) = \sum_i a_i\ \psi(\underline{P}_i\uparrow)\psi(-\underline{P}_i\downarrow) \qquad 2.15$$

where

$$|a_i|^2$$

gives the probability of finding the electrons at any instant with individual momenta $\underline{P}_i$.

$\Phi(r_1,r_2)$ describes what is called a "Cooper pair". The total energy of the two electrons is

$$W = \text{potential energy} + \text{kinetic energy}$$

$$= 2 \sum_i |a_i|^2 \ \frac{P_i^2}{2m} \quad . \qquad 2.16$$

The states available for the two electrons are those with $\underline{P} > \underline{P}_F$. If $\Phi(r_1, r_2)$ is normalised,

$$\sum |a_i|^2 = 1$$

and the kinetic energy $> 2P_F^2/2m = 2\varepsilon_F$ where suffix F refers to the Fermi surface.

(i) The Ground State and the Energy Gap

The electron-electron interaction is attractive when their energies $\varepsilon(\underline{k})$, $\varepsilon(\underline{k}-\underline{q})$ are nearly equal and the matrix element is negative. The interaction is repulsive when their energy difference is less than $\hbar\omega_q$ i.e.

$$|\varepsilon(\underline{k}) - \varepsilon(\underline{k}-\underline{q})| < \hbar\omega_q$$

and the matrix element is of the form

$$M(\underline{k},\underline{k}-\underline{q}) = \frac{\hbar\omega^2}{\{\varepsilon(\underline{k}) - \varepsilon(\underline{k}-\underline{q})\}^2 - (\hbar\omega)^2} \qquad 2.17$$

with a singularity at $\varepsilon(\underline{k}) - \varepsilon(\underline{k}-\underline{q}) = \hbar\omega$.

The BCS criterion for superconductivity is that the phonon interaction dominate over the Coulomb interaction and define the effective matrix element as

$$-V \equiv <- \frac{2|M_k|^2}{\hbar\omega_k} + \frac{4\pi e^2}{\kappa_{eff}^2}> \; < \; 0 \qquad 2.18$$

where κ_{eff} is the effective momentum exchange.

The electron pairing idea is extended to a large number of electrons and in the ground state all the Cooper pairs should have momentum zero. The ground superconducting state will be formed of those paired states which have the largest number of transitions among them. For pairing between electrons with equal and opposite spin, the reduced Hamiltonian is

$$H_{red} = T + H_{int}$$

$$= 2 \sum_{k} \varepsilon_k a_k^{\dagger} a_k - \sum_{k,k'} V_{kk'} a_{k'}^{\dagger} a_k \qquad 2.20$$

where T is the kinetic energy term, H_{int} is the interaction energy term, $V_{kk'}$ is the interaction matrix element, $a_k^{\dagger}$ and a_k are creation and annihilation operators. The BCS ground state is given by

$$|\Phi_o\rangle = \prod_{k} (u_k + v_k a_{k\uparrow}^{\dagger} a_{-k\downarrow}^{\dagger}) |0\rangle \qquad 2.21$$

where $|0\rangle$ is the vacuum state with no electrons. u_k and v_k are variational coefficients satisfying the normalization condition

$$u_k^2 + v_k^2 = 1 \quad . \qquad 2.22$$

In this state there are no unpaired electrons. v_k^2 is the probability of finding a pair in the pair state

$(\underline{k}\uparrow,-\underline{k}\downarrow)$ and u_k^2 is the probability of this pair state being empty. $|\Phi_o\rangle$ becomes the normal Fermi state when

$$\left.\begin{aligned} v_k &= 1 \\ u_k &= 0 \end{aligned}\right\} \quad \text{for} \quad k < k_F \qquad 2.23a$$

$$\left.\begin{aligned} v_k &= 0 \\ u_k &= 1 \end{aligned}\right\} \quad \text{for} \quad k > k_F \qquad 2.23b$$

Introducing equivalent parameters

$$v_k^2 = h_k$$

$$u_k^2 = 1 - v_k^2 = 1 - h_k \qquad 2.24$$

$$b_k^\dagger = a_{\underline{k}\uparrow}^\dagger \, a_{-\underline{k}\downarrow}^\dagger$$

$$b_k = a_{\underline{k}\uparrow} \, a_{-\underline{k}\downarrow} \qquad 2.25$$

(2.21) becomes

$$|\Phi_o\rangle = \prod_k [(1 - h_k)^{\frac{1}{2}} + h_k^{\frac{1}{2}} \, b_k^\dagger]|0\rangle \quad . \qquad 2.26$$

The condensation energy corresponding to H_{red} is

$$W_c = 2 \sum \varepsilon_k h_k - \sum \{h_k(1-h_k)h_{k'}(1-h_{k'})\}^{\frac{1}{2}} V_{kk'}$$

2.27

W_c is a maximum when

$$\frac{\partial W_c}{\partial h_k} = 0 \quad . \tag{2.28}$$

(2.27) and (2.28) give the results

$$v_k^2 = \frac{1}{2}\left(1 - \frac{\varepsilon_k}{\sqrt{(\varepsilon_k^2 + \Delta_k^2)}}\right) = h_k$$

$$u_k^2 = \frac{1}{2}\left(1 + \frac{\varepsilon_k}{\sqrt{(\varepsilon_k^2 + \Delta_k^2)}}\right) = 1 - h_k \tag{2.29}$$

where

$$\Delta_k = \sum_{k'} V_{kk'} u_{k'} v_{k'} = \sum_{k'} \frac{V_{kk'} \Delta_{k'}}{2E_{k'}}$$

$$= \sum_{k'} V_{kk'} \{h_{k'}(1 - h_{k'})\}^{\frac{1}{2}} \quad . \tag{2.30}$$

Δ_k turns out to be the energy gap parameter for the k^{th} electron. Introducing another notation

$$E_k^2 = \Delta_k^2 + \varepsilon_k^2 \quad . \tag{2.31}$$

Under the assumptions that $V_{kk'}$ can be replaced by an average value V for $|\varepsilon_k| < \hbar\omega_c$ where ω_c is the phonon cut off frequency;

$$\Delta_k \simeq \text{constant} = \Delta \qquad \text{for} \qquad |\varepsilon_k| < \hbar\omega_c$$

and $$\Delta_k = 0 \qquad \text{for} \qquad |\varepsilon_k| > \hbar\omega_c \ .$$

Replacing the summation by an integral over the density of states N(E) (2.30) gives

$$\frac{1}{N(0)V} = \int_0^{\hbar\omega_c} \frac{d\varepsilon}{(\varepsilon^2 + \Delta^2)^{\frac{1}{2}}} \qquad 2.32$$

where N(0) is the density of states at the Fermi level. Integrating (2.32) gives

$$\Delta = \frac{\hbar\omega_c}{\sinh\left(\frac{1}{N(0)V}\right)} \quad . \qquad 2.33$$

In the weak coupling $N(0)V << 1$ and

$$\Delta \simeq 2\hbar\omega_c e^{-1/N(0)V} \quad . \qquad 2.34$$

Since excited single particle states are produced in pairs, the minimum energy for allowed excitation is 2Δ.

(ii) Density of States

In a BCS superconductor the density of excited states is

$$\frac{dN(E)}{dE} = \frac{dN(\varepsilon)}{d\varepsilon}\frac{d\varepsilon}{dE} = N(0)\frac{d\varepsilon}{dE}$$

but

$$E = (\Delta^2 + \varepsilon^2)^{\frac{1}{2}}$$

$$\frac{dN(E)}{dE} = N(0)\frac{|E|}{(E^2 - \Delta^2)^{\frac{1}{2}}} \qquad |E| \geq \Delta$$

$$= 0 \qquad |E| < \Delta \qquad 2.35$$

Figure 2.3 shows the behaviour of equation 2.35. Experimental results on tunneling by Giaever et al (1962), Adler and Rogers (1963), Rowell et al (1963) are in good agreement between measurements on Al, Pb, Sn and the BCS density of states.

(iii) Critical Temperature

The energy gap is not a constant but decreases as the temperature rises. An electron in state ($\underline{P}\uparrow$) without a partner in state ($-\underline{P}\downarrow$) prevents the pair state ($\underline{P}\uparrow$, $-\underline{P}\downarrow$) from being available to the Cooper pairs and the pair interaction energy is decreased because the number of scattering events in which they can participate is decreased; and this implies a decrease in the energy gap. As the temperature rises, the number of free like broken up Cooper pairs i.e. quasi-particles, increases and the energy gap continues to fall until a temperature is reached at which the energy gap is zero. This temperature is called the critical temperature T_c.

Evaluation of (2.30) gives

$$\Delta_k = \sum_{k'} V_{kk'}[h_{k'}(1 - h_{k'})]^{\frac{1}{2}} (1 - 2f_{k'}) \qquad 2.36$$

where

$$E_k = (\Delta_k^2 + \varepsilon_k^2) = - kT \ln\left(\frac{f_k}{1 - f_k}\right) \quad .$$

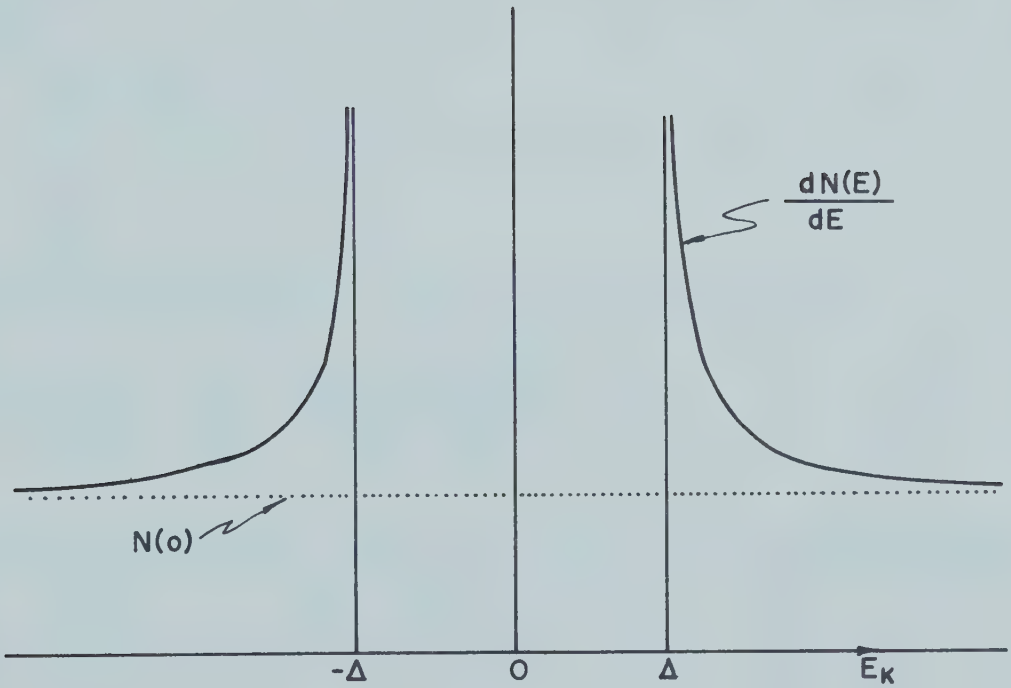

Figure 2.3

Density of states in the BCS theory.

$$f_k = \frac{1}{e^{E_k/kT} + 1} = f(E_k)$$

is the Fermi function. Substituting for h_k we get

$$\Delta_k = \sum V_{k'k} \frac{\Delta_{k'}}{2E_{k'}} \left(1 - \frac{2}{(e^{E_k/kT} + 1)}\right)$$

putting

$$\Delta_k = \Delta_{k'} = \Delta$$

$$V_{kk'} = V$$

and using the integral instead of the summation,

$$\frac{1}{N(0)V} = \int_0^{\hbar\omega_c} \frac{\tanh\left[\frac{(\varepsilon^2 + \Delta^2)^{\frac{1}{2}}}{2kT}\right]}{(\varepsilon^2 + \Delta^2)^{\frac{1}{2}}} \, d\varepsilon \quad . \qquad 2.36'$$

(2.36)' is equivalent to (2.32) at T = 0°K and determines $\Delta(0)$. At T_c, $\Delta \to 0$, and for $T > T_c$, (2.36)' has no solution but the metal is normal with no energy gap

$$\frac{1}{N(0)V} = \int_0^{\hbar\omega_c} \frac{\tanh\left(\frac{\varepsilon}{2kT_c}\right)}{\varepsilon} \, d\varepsilon \qquad \text{at } \Delta = 0 \; . \qquad 2.37$$

For weak coupling,

$$kT_c = 1.14\, \hbar\omega_c \, e^{-1/N(0)V} \quad . \qquad 2.38$$

From (2.34) and (2.38) at T = 0,

$$2\Delta(0) = 3.5\, kT_c \quad . \qquad 2.39$$

Near the critical temperature T_c ,

$$\Delta(T) \simeq 3.2\ kT_c\ (1 - \frac{T}{T_c})^{\frac{1}{2}} . \qquad 2.40$$

The energy gap as a function of temperature is shown in figure 2.4.

(iv) (a) The Critical Field

The critical field satisfies the relation

$$G_n(0) - G_s(0) = \frac{1}{8\pi} H_c^2 \qquad 2.41$$

where $G_n(0)$ and $G_s(0)$ are the Gibb free energy densities of the normal and superconducting phases. At T = 0°K, $G_n(0) - G_s(0)$ is equal to the difference between the internal energy densities in the normal and superconducting states. According to the BCS theory this is the total binding energy of the Cooper pairs. Equation (2.41) then reads

$$\frac{1}{8\pi_c} H_c^2 = G_n(0) - G_s(0) = \frac{1}{2} N(0)(\Delta(0))^2$$

$$= \frac{1}{2} N(0) (\frac{3.5}{2} k)^2 T_c^2$$

$$\frac{H_c^2}{T_c^2} = \pi N(0) (3.5)^2 k^2 = 5.87\ \gamma \qquad 2.42$$

where

$$\gamma = \frac{2}{3} \pi^2 N(0) k^2 .$$

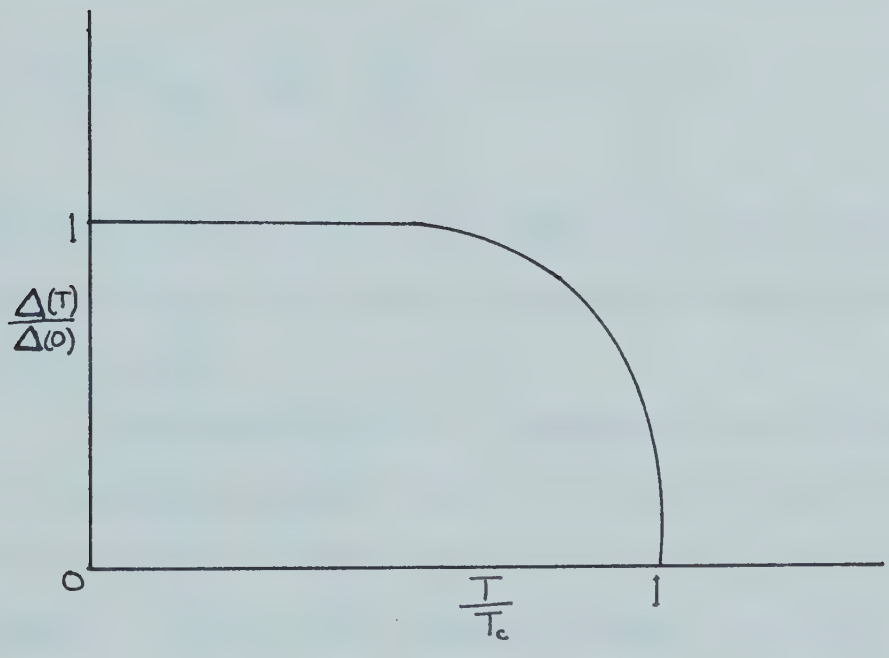

Figure 2.4

Temperature dependence of the energy gap in a superconductor.

(b) Size Effect on the Critical Field

When one of the dimensions of a superconductor is of the order of the penetration depth, the critical magnetic field is much higher than that of the bulk specimen.

In an external field H_e , a superconductor acquires a magnetization $M(H_e)$ and becomes normal when

$$\int_0^{H_e} M(H_e)\, dH_e = \frac{H_c^2}{8\pi} \quad . \qquad 2.43$$

Equation (2.43) represents the area under the curve of figure 2.5 in the case of a spherical superconductor, Lynton (1962).

The susceptibility χ determines the initial slope of the magnetization curve. A lower χ implies the curve has to go to a higher critical field H_s for the small sample. If the curve remains linear up to H_s ,

$$\frac{H_s^2}{H_c^2} = \frac{\chi_o}{\chi} \qquad 2.44$$

and

$$\frac{H_s}{H_c} = 1 + \frac{\lambda}{2a} \qquad \text{for} \quad a >> \lambda_o$$

$$\frac{H_s}{H_c} = \sqrt{3}\ \frac{\lambda}{a} \qquad \text{for} \quad a << \lambda_o \quad . \qquad 2.45$$

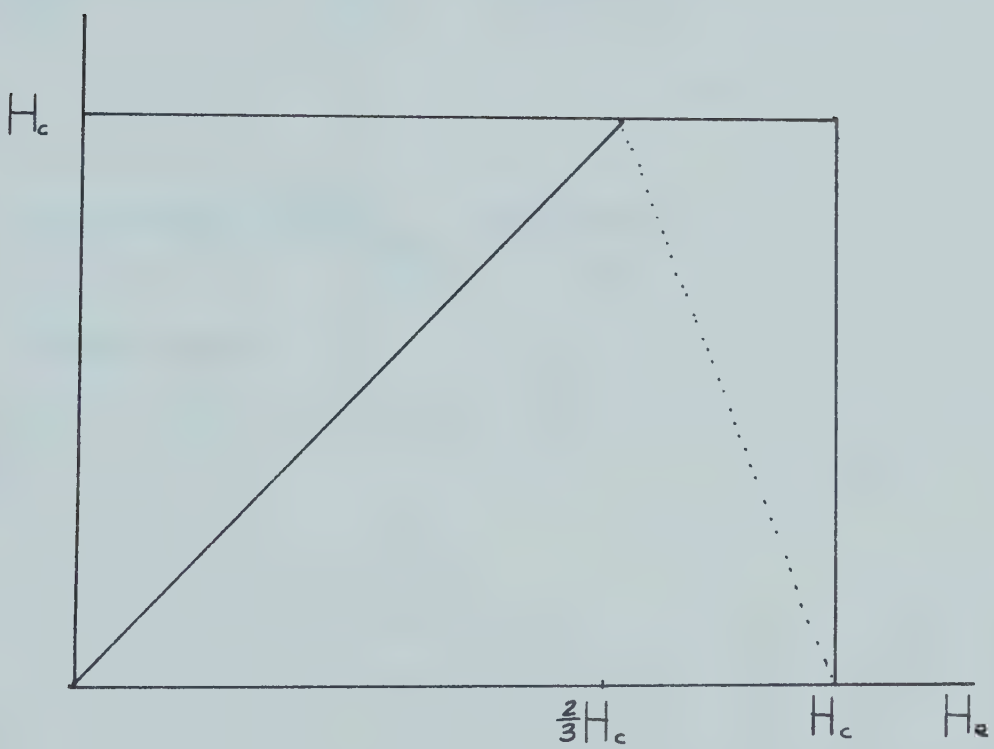

Figure 2.5

Magnetization curve of a spherical superconductor.

Because of the addition terms in the free energy equation (2.41), the penetration depth increases and the critical field becomes much higher. For a thickness of 2a, $a << \lambda_o$,

$$\left(\frac{H_s}{H_c}\right)^2 = 6\left(\frac{\lambda_o}{a}\right)^2 - \frac{7}{10}\kappa^2 + \frac{11}{1400}\left(\frac{a}{\lambda_o}\right)^2$$

where

$$\kappa = 2.16 \times 10^7 \left|\frac{dH_c}{dT}\right|_{T=T_c} T_c \lambda_L^2(0) \ .$$

When κ is very small

$$\frac{H_s}{H_c} \simeq \sqrt{6} \ \frac{\lambda_o}{a} \ . \qquad 2.46$$

CHAPTER 3

MODELS OF TUNNELING

Giaever (1960a,b) demonstrated experimentally that a current can pass between two metals separated by a thin insulating layer. This work was extended by Nicol et al (1960), Giaever and Fisher (1961), Giaever and Megerle (1961) for the case where one or both of the metals are superconducting.

The foundation for the theory of tunneling was laid by Bardeen (1961) and further treatment has been made by Cohen et al (1962) and Prange (1963). Adler (1963) has given a good account of these theories.

A. Simple Model of Tunneling

If two metals are separated by a thin insulating layer, figure 3.1, electrons can tunnel through from one metal to the other. At low voltages, the tunnel current is ohmic. In this picture the transmission coefficient of an electron to go through the potential barrier varies as $\exp\{-\frac{2t}{\hbar}(m\phi)^{\frac{1}{2}}\}$ where m is the electron mass, $\hbar$ Planck's constant, t the insulating layer thickness and ϕ the work function.

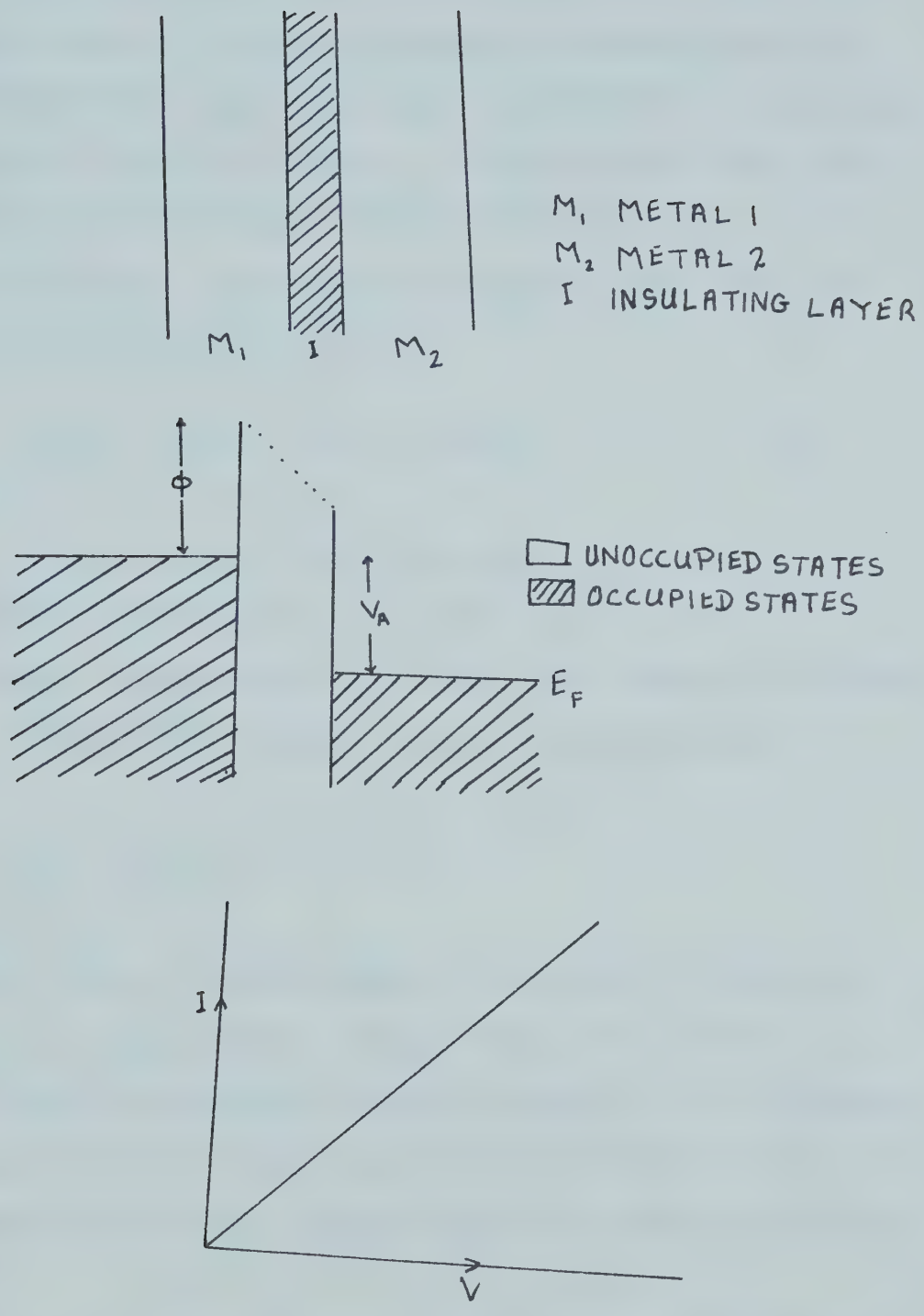

Figure 3.1

Tunneling between two metals seperated by a thin insulating layer.

The probability that an electron will tunnel from the left metal to the right metal is proportional to the probability, f_k, that there is initially an electron in the left metal in state $\underline{k}$. This electron can tunnel to the right metal into state $\underline{k}'$ only if state $\underline{k}'$ is initially empty. According to Fermi's rule, the transition probability is given by

$$P_{\underline{k}_i \to \underline{k}_f} = \frac{2\pi}{\hbar} |M|^2 f_i (1 - f_f) N_f \qquad 3.1$$

where M is a matrix element for the transition, f_i and f_f are the probabilities that the initial and final states are occupied and N_f is the final density of states.

The partial current, $I_{L \to R}$, is proportional to

$$\sum_{\underline{k}_i, \underline{k}_f} N_1 N_2 f_i (1 - f_f) |M|^2$$

where N_1 and N_2 are the density of states in the left and in the right metals respectively. We assume that the tunneling electrons impinge normally on the boundary and that there is a one-to-one correspondence between the specification of states in the left metal and right metal.

The net current across the barrier when voltage V is applied is

$$I = I_{L\to R} - I_{R\to L}$$

$$= \frac{4\pi e}{\hbar} \int_{-\infty}^{\infty} |M|^2 \{N_1(E) f(E) (1 - f(E+eV)) N_2(E+eV)$$

$$- N_2(E+eV) f(E+eV) (1 - f(E)) N_1(E) \} dE \qquad 3.2$$

where E is the energy measured from the Fermi level and f is the Fermi function.

When $eV << E_F$, where E_F is the Fermi energy, M is taken to be independent of eV.

At $T = 0°K$, $f(E) = 0 : E > 0$; $f(E+eV) = 0 : E < -eV$

$= 1 : E < 0$ $= 1 : E > eV$.

It is further assumed that near the Fermi level the density of states is constant. Equation 3.2 can be written as

$$I = \frac{4\pi e}{\hbar} |M|^2 \int_{-\infty}^{\infty} N_1(E) N_2(E+eV) \{f(E) - f(E+eV)\} dE$$

$$= \frac{4\pi e}{\hbar} |M|^2 \left(\int_{-\infty}^{\infty} N_1(E) N_2(E+eV) dE - \int_{-\infty}^{eV} N_1(E) N(E+eV) dE \right)$$

$$= \frac{4\pi e}{\hbar} |M|^2 \int_{+eV}^{0} N_1(E) N_2(E+eV) dE \quad . \qquad 3.3$$

Put

$$N_1(E) = Q_1(E) N_{1n}(E)$$

$$N_2(E) = Q_2(E) N_{2n}(E) \qquad 3.4$$

where in the normal state $Q_1(E) = Q_2(E) = 1$ and also eV is very small. Now the current can be expanded about the Fermi level.

$$I = \frac{4\pi e}{\hbar} |M|^2 \int_{eV}^{0} Q_1(E)Q_2(E+eV)\{N_{1n}(0) + E(\frac{\partial N_{1n}}{\partial E})_{E=0} + \ldots\} \times$$

$$\{N_{2n}(eV) + E(\frac{\partial N_{2n}}{\partial E})_{E=eV} + \ldots\}dE \quad . \qquad 3.5$$

(a) Normal-Normal case, I_{nn}

$Q_1(E) = Q(E+eV) = 1$ and the energy densities do not vary very much with E.

$$I_{nn} = \frac{4\pi e}{\hbar} |M|^2 \left(\int_{eV}^{0} Q_1(E)Q(E+eV)dE \right) N_{1n}(0)N_{2n}(0)$$

$$= \frac{4\pi e^2}{\hbar} |M|^2 N_{1n}(0)N_{2n}(0)V \quad . \qquad 3.6$$

Figure 3.2a shows the densities of states at zero and non-zero temperatures and the I-V characteristics.

(b) Normal-Superconducting case, I_{ns}

$$Q_1(E) = \text{Re}\left(\frac{|E|}{\sqrt{(E^2 - \Delta^2)}}\right) = \frac{|E|}{\sqrt{(E^2 - \Delta^2)}} \quad \text{for} \quad E > \Delta$$

$$= 0 \quad \text{otherwise}$$

$$Q_2(E+eV) = 1$$

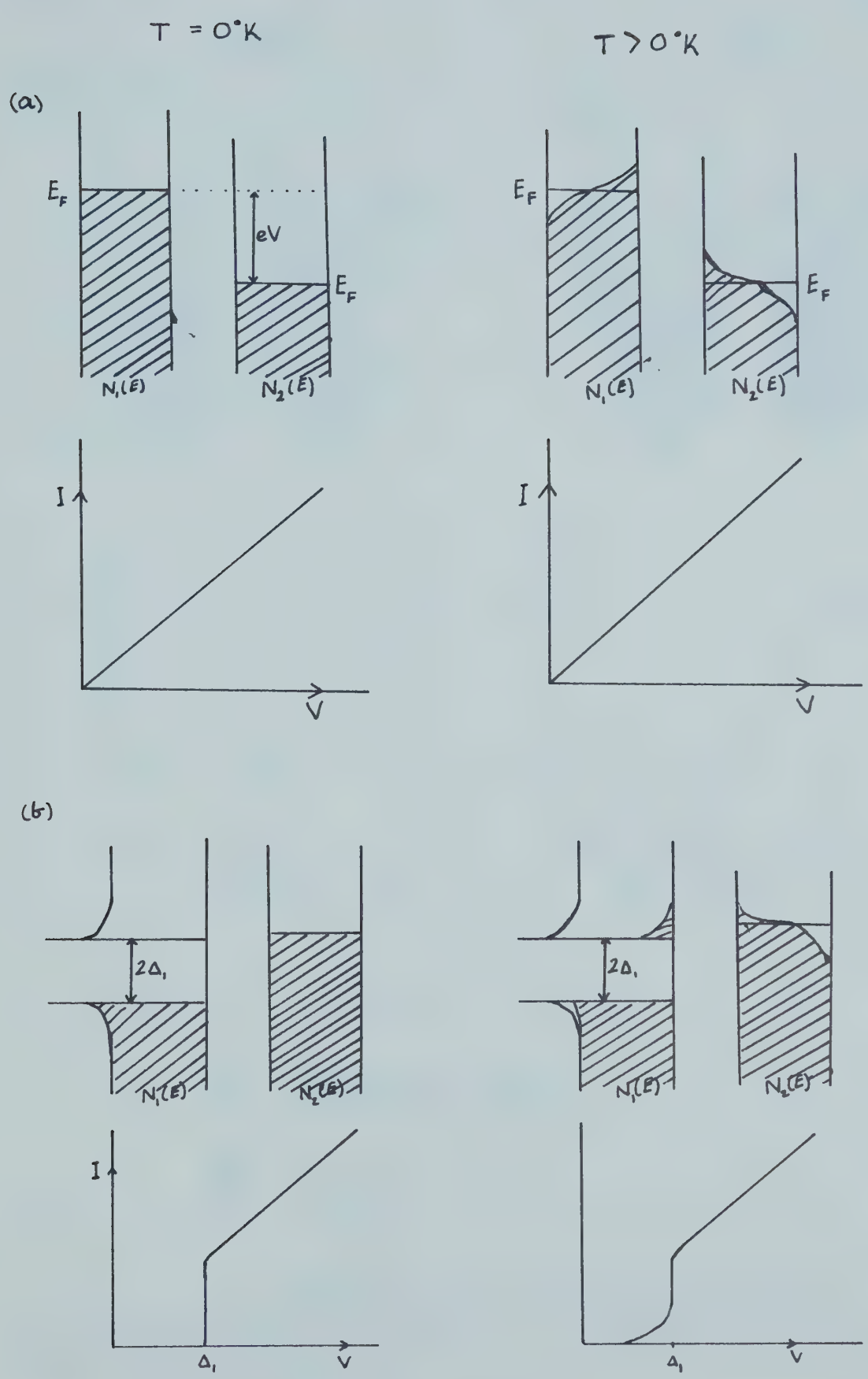
T = 0°K
T > 0°K
(a)
E_F
eV
E_F
$N_1(E)$
$N_2(E)$
I
V
(b)
$2\Delta_1$
$N_1(E)$
$N_2(E)$
I
Δ_1
V

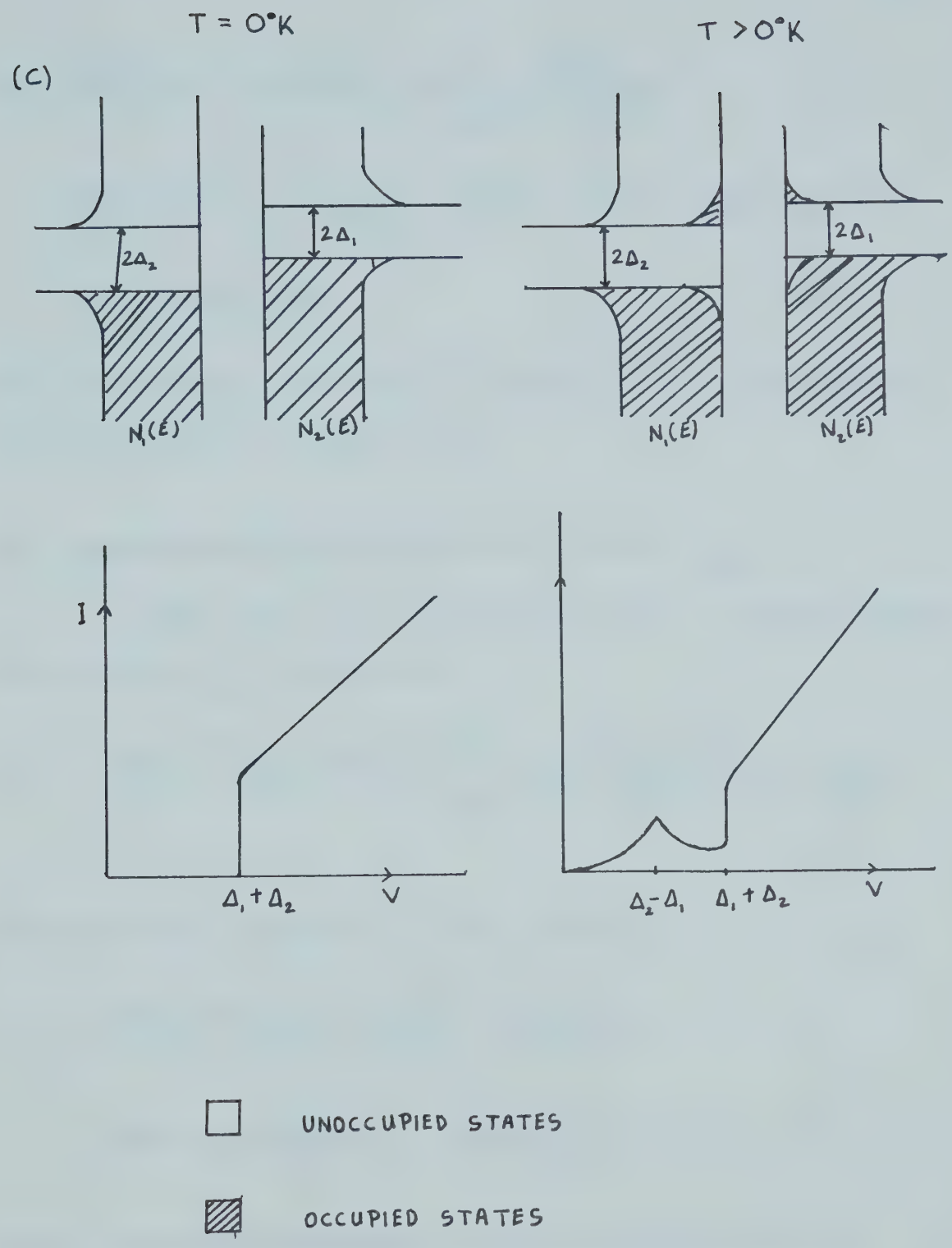

Figure 3.2
Energy diagrams illustrating the density of states near the Fermi level, occupation of states and current-voltage characteristics in
(a) normal-normal case
(b) normal-superconducting case
(c) superconducting-superconducting case.

$$I_{ns} = \frac{4\pi e}{\hbar} |M|^2 N_{1n}(0)N_{2n}(0) \int_{-eV}^{0} \frac{E\, dE}{(E^2 - \Delta^2)^{\frac{1}{2}}}$$

$$= \frac{4\pi}{\hbar} |M|^2 N_{1n}(0)N_{2n}(0)((eV)^2 - \Delta^2)^{\frac{1}{2}} \quad \text{for } |eV| > \Delta$$

$$= 0 \quad \text{otherwise} \quad . \qquad 3.7$$

The corresponding density of states and I-V characteristics are shown in figure 3.2b.

(c) Superconducting-Superconducting case, I_{ss}

In this case $Q_1(E)$ and $Q_2(E+eV)$ are no longer simple. The current I_{ss} is given by

$$I_{ss} = \frac{4\pi e}{\hbar} |M|^2 N_{1n}(0)N_{2n}(0) \int_{-eV}^{0} \frac{E(E+eV)dE}{[(E^2 - \Delta_1^2)(E+eV)^2 - \Delta_2^2]^{\frac{1}{2}}} \qquad 3.8$$

In the final integration (3.8) reduces to

$$I_{ss} = \frac{4\pi e}{\hbar} |M|^2 N_n^2(0) \left[\frac{(eV)^2}{eV+2\Delta} K\left(\frac{eV-2\Delta}{eV+2\Delta}\right) + (eV+2\Delta)\left[E\left(\frac{eV-2\Delta}{eV+2\Delta}\right) - K\left(\frac{eV-2\Delta}{eV+2\Delta}\right)\right]\right] \qquad 3.9$$

where K and E are complete elliptic integrals of the first kind. Adler (1963) has carried out a rigorous derivation and calculation of (3.9). The density of states and I-V characteristics are shown in figure 3.2c.

At 0°K I_{ss} is zero until the applied voltage is equal to $\Delta_1 + \Delta_2$ at which voltage it will increase sharply approaching I_{nn} at higher voltages. At non-zero temperature, a small current will flow at small applied voltages due to thermally excited electrons above the energy gaps. This current will increase up to $V = \Delta_2 - \Delta_1$, $(\Delta_2 > \Delta_1)$ and at $V > \Delta_2 - \Delta_1$ it will decrease because the same number of electrons will be available for tunneling as in the $V < \Delta_2 - \Delta_1$ range. This decrease will continue until $V = \Delta_2 + \Delta_1$ and at that voltage the current will rise sharply.

B. The Modified Tunneling Model

The effective Hamiltonian is given by

$$H = H_1 + H_2 + H_T \qquad 3.10$$

where H_1 and H_2 are the Hamiltonians for the left metal and the right metal respectively and H_T is the electron transfer Hamiltonian given by

$$H_T = \sum_{kk's} (M_{kk'} a^{*(2)}_{k's} a^{(1)}_{ks} + M_{k'k} a^{*(1)}_{ks} a^{(2)}_{k's}) \qquad 3.11$$

where s refers to spin.

Schrieffer (1963) considered H_T as a small perturbation. The rate of electron transfer from 1 to 2 is

$$\omega_{1\to 2} = 2\pi \sum_{\alpha,\beta} |\langle\alpha_1|\langle\beta_2| \sum_{kk's} M_{kk'} a^{*(2)}_{k's} a^{(1)}_{ks} |0_1\rangle|0_2\rangle|^2 \times \delta(\varepsilon_\alpha + \varepsilon_\beta - V) \qquad 3.12$$

when the electrons potential decrease by V in moving from 1 to 2. $|\alpha_1\rangle$ and $|\beta_2\rangle$ are eigenstate vectors of H_1 and H_2 respectively. ε_α and ε_β are energy differences between $|0_1\rangle$ and $|\alpha_1\rangle$, $|0_2\rangle$ and $|\beta_2\rangle$ respectively.

At 0°K electrons cannot tunnel from 2 to 1 because of the conservation of energy. The current I(V) is proportional to the rate of transfer of electrons:

$$I(V) \propto \int_0^V N_{T+}^{(2)}(E)\, N_{T-}^{(1)}(V-E)\, dE \qquad 3.13$$

where

$$N_{T+}^{(2)}(E) = \sum_{k,\beta} |\langle \beta_2 | a_k^*, | 0_2 \rangle|^2\, \delta(\varepsilon_\beta - E) \qquad 3.14$$

$$N_{T-}^{(1)}(E) = \sum_{k,\alpha} |\langle \alpha_1 | a_k | 0_1 \rangle|^2\, \delta(\varepsilon_\alpha - E) \qquad 3.15$$

(+) and (-) refer to "electrons" and "holes" respectively. Using Green's function, Schrieffer reduced (3.14) and (3.15) to

$$N_{T\pm}(E) = N(0)\ \mathrm{Re}\ \left\{\frac{E}{(E^2 - \Delta^2(E))^{\frac{1}{2}}}\right\} \qquad 3.16$$

Differentiating (3.13) with respect to V, for the normal-superconductor case,

$$\sigma = \frac{\sigma_s}{\sigma_n} = \frac{(\frac{dI_s}{dV})}{(\frac{dI_n}{dV})} = \mathrm{Re}\ \left\{\frac{V}{(V^2 - \Delta^2(V))^{\frac{1}{2}}}\right\} \qquad 3.17a$$

σ is called the dynamical conductance. From (2.35),

$$\sigma = \frac{N(E)}{N(0)} = \text{Re}\left\{\frac{V}{(V^2 - \Delta^2(V))^{\frac{1}{2}}}\right\} \quad . \qquad 3.17b$$

The process thus described is illustrated in figure 3.3. In (3.3a) an electron in $\underline{k}\uparrow$ below the Fermi level in the normal tunnels through the barrier to state $\underline{k}'\uparrow$ above the Fermi level in the superconductor. A hole is left behind resulting in an excitation energy $\varepsilon_\alpha = |\varepsilon_k|$ for metal 1. Due to a quasiparticle in $\underline{k}'\uparrow$, there is an excitation energy $\varepsilon_\beta = E_{k'} = (\varepsilon_{k'}^2 + \Delta_{k'}^2)^{\frac{1}{2}}$ in metal 2. This process will occur only if the pair state $(\underline{k}'\uparrow, -\underline{k}'\downarrow)$ is initially empty. Energy is conserved if $|\varepsilon_k| + E_{k'} = V$. In figure (3.3b) the particle goes in state $\underline{k}''$ below the Fermi level in the superconductor. If Δ_2 is constant, $\varepsilon_{k'} = -\varepsilon_{k''}$.

In figure (3.3c) where both metals are superconducting, an electron in $\underline{k}\uparrow$ can tunnel to either $\underline{k}'\uparrow$ or $\underline{k}''\uparrow$, or an electron in $\bar{\underline{k}}\uparrow$ can tunnel to the same final states $\varepsilon_{\underline{k}} = -\varepsilon_{\underline{k}}$. The current this time begins at $V = \Delta_1 + \Delta_2$ at 0°K.

C. The Capacitor Model

In an attempt to explain the observed zero-bias resistance anomalies, Giaever and Zeller (1968) introduced a capacitor model. Mezei (1971) has tried to

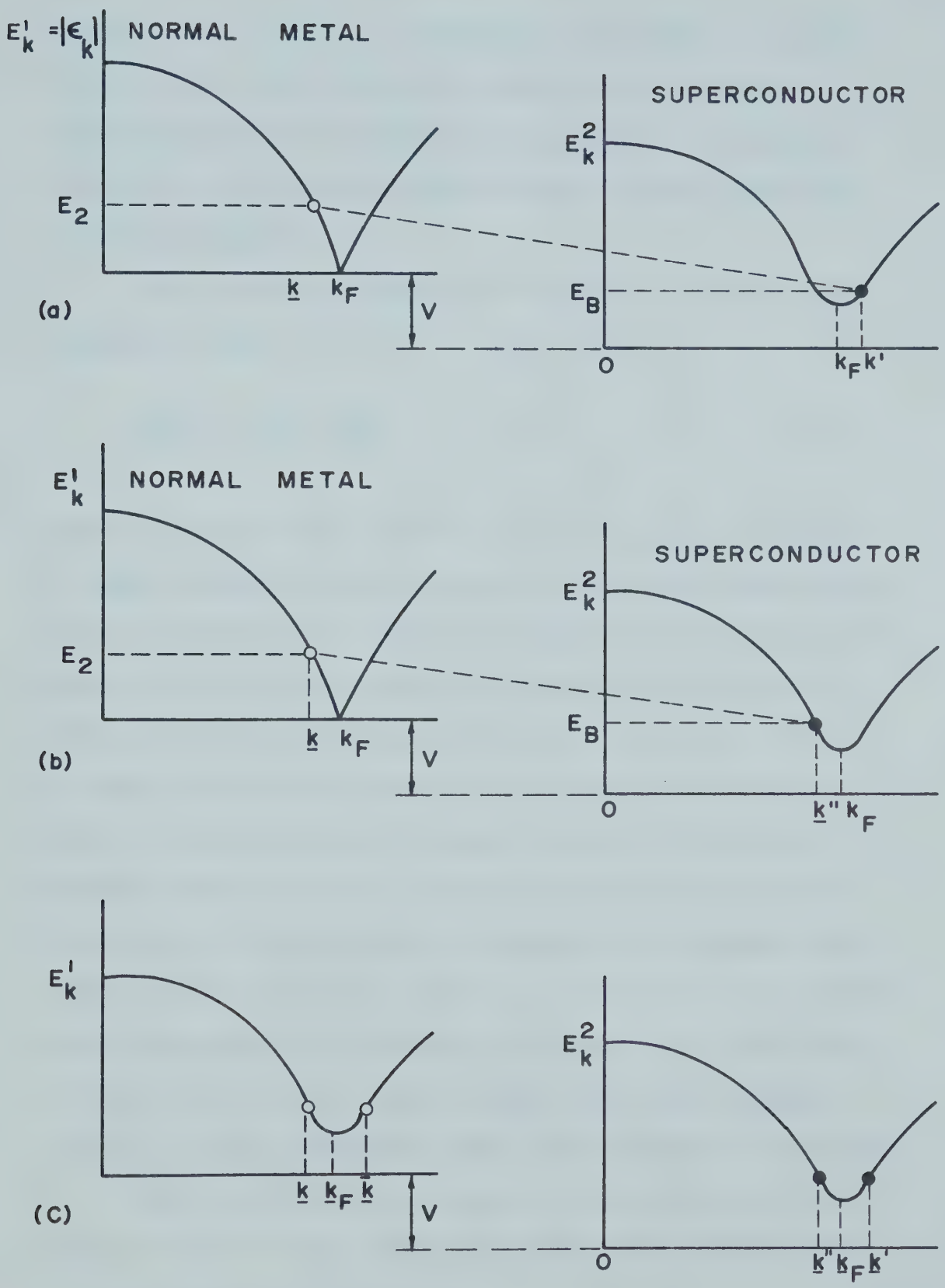

Figure 3.3
Electron transfer processes in
(a) n-s with the particle going to state $\underline{k}'$ above $\underline{k}_F$
(b) n-s with the particle going to state $\underline{k}''$ below $\underline{k}_F$
(c) s-s with two possibilities of going to $\underline{k}'$ or $\underline{k}''$

explain this model in a microscopic picture. Townsend et al (1971) have followed Giaever-Zeller argument except that they discussed the dependence of conductivity on zero bias and temperature at both zero and non-zero temperatures.

The potential energy of a sphere of radius r and carrying charge e is

$$\frac{1}{2}\frac{Q^2}{C} = \frac{1}{2}\frac{e^2}{r}\frac{1}{4\pi\varepsilon_o} \qquad 3.18$$

where $Q = e$ and the capacitance $C = 4\pi\varepsilon_o r$. If contact is made between the two sides of a parallel plate capacitor, figure (3.4), which has capacitor plates made of metals with different work functions, electrons are exchanged until the Fermi levels are aligned. If one of the plates is of a small finite size, exact alignment is not possible; alignment occurs in discrete voltage steps $\Delta V = e/C$. At equilibrium the number of electrons on the particle is closest to alignment, the difference in voltage being $|V_D| < e/2C$. At low temperatures the number of electrons is fixed. The two films and any one particle can exchange electrons, figure (3.5a), through tunneling until equilibrium is attained.

When the voltage is applied, electrons can flow from one side of the junction to the other side by any of the following processes:

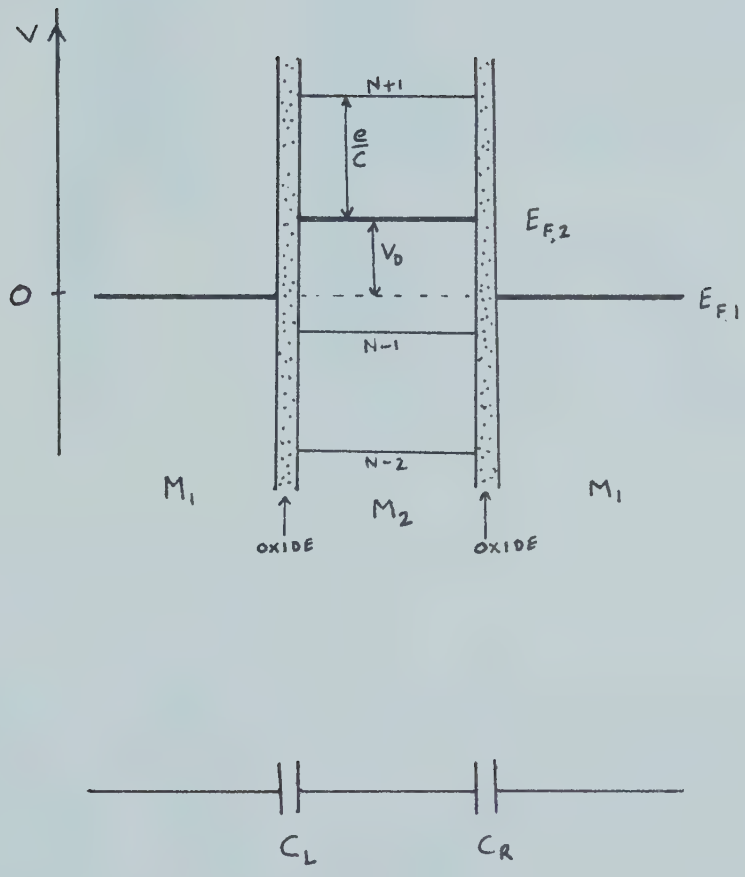

Figure 3.4

Particles embedded in oxide seperating two metal films represented as two capacitors in series.

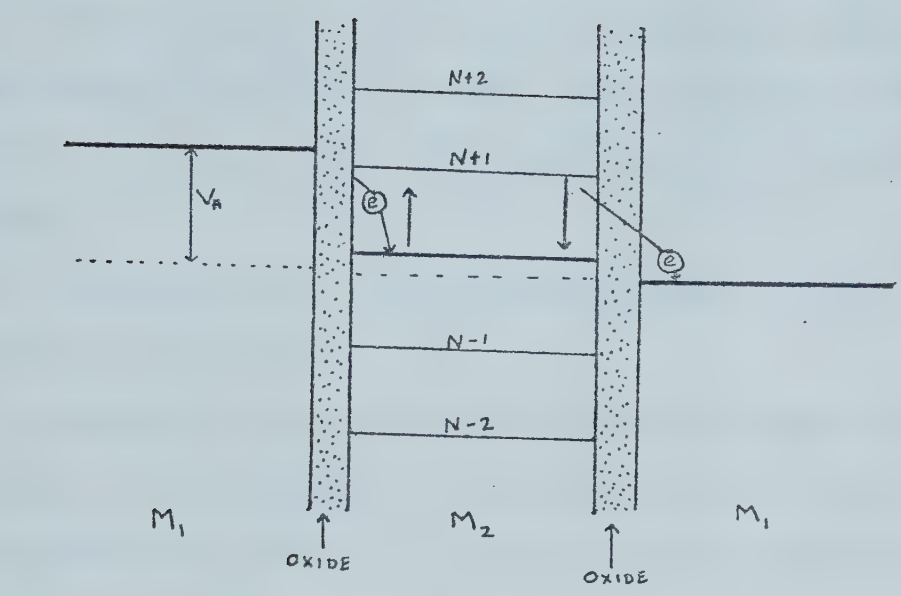

(a)

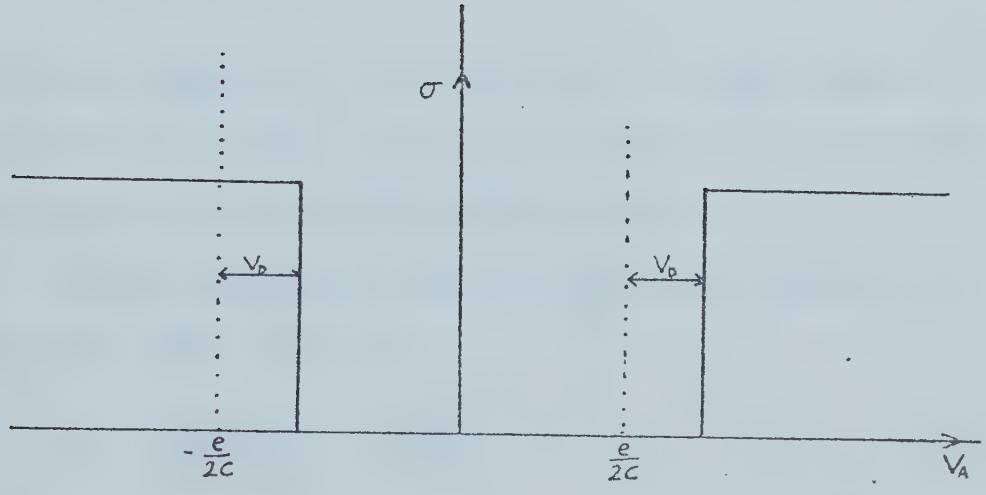

(b)

Figure 3.5

(a) Particle excited levels

(b) Voltage dependence of the conductance

I. Direct tunneling through the metal oxide as in a usual metal-metal oxide-metal junction. This gives a constant voltage temperature independent conductivity.

II. Tunneling from one film to a particle localising the electron there for a short time and then tunneling out to the other film. What follows will be about this process.

III. Tunneling as in the second process but not localising the electron.

Process II requires an activation energy which in turn is responsible for zero bias resistance peak. The activation energy E is equal to the energy difference between the initial and final states.

$$E = \frac{1}{2} \left(\frac{e}{C} \pm V_D\right)^2 C - \frac{1}{2} V_D^2 C$$

The level spacing in the particle is assumed much less than E and therefore the spacing effects are negligible. E is purely a classical Coulomb energy.

In the pictorial representation of figure (3.4), the total capacitance is

$$C' = \frac{C_R C_L}{C_R + C_L} = \frac{C_R C_L}{C} \quad ;$$

if M_2-oxide is much thicker than M_1-oxide, $C_L >> C_R$ so that the applied voltage appears between the particle

and the right film. When a particle tunnels from left to the particle, charge flow is opposed by a polarising charge

$$e \frac{C_L}{C_L+C_R}$$

due to the left capacitor. The net charge is

$$e - \frac{eC_L}{C_L+C_R} = \frac{eC_R}{C_L+C_R} \quad .$$

Battery energy is

$$qV = \frac{eC_L V}{C_L+C_R} = \frac{eC_L V}{C} \quad .$$

For current to flow the applied voltage must be greater than the activation energy, i.e.

$$\frac{eVC_L}{C} \geq \frac{1}{2}C\left(\frac{e}{C} \pm V_D\right)^2 - \frac{1}{2} V_D^2 C = \frac{e^2}{2C} \pm eV_D$$

$$V \geq \frac{C}{C_L} \left(\frac{e}{2C} \pm V_D\right) \quad .$$

With the assumption $C \simeq C_L >> C_R$, the condition for current flow becomes

$$|V| > \frac{e}{2C} + V_D \qquad \text{for} \qquad V > 0$$

$$|V| > \frac{e}{2C} - V_D \qquad \text{for} \qquad V < 0 \quad .$$

Therefore for a single particle,

$$\sigma_D(V) = 0 \quad \text{if} \quad -\frac{e}{2C} + V_D < V < \frac{e}{2C} + V_D$$

$$= \text{constant} \quad \text{otherwise} . \qquad 3.19$$

Figure (3.5b) illustrates equation (3.19). We assume that for a set of particles of given capacitance C, V_D is uniformly distributed in the range $-e/2C < V < e/2C$. The average conductivity for this set of particles is

$$\langle\sigma(V)\rangle = \frac{\int_{-e/2C}^{e/2C} \sigma_D(V)\,dV_D}{\int_{-e/2C}^{e/2C} dV_D} = \frac{C}{e}\int_{-e/2C}^{e/2C} \sigma_D(V)\,dV_D \qquad 3.20$$

Define

$$V_c = \frac{e}{2C} + V_D \qquad 3.21$$

(3.20) becomes

$$\langle\sigma(V)\rangle = \frac{C}{e}\int_0^{e/C} \sigma_D(V)\ dV_c \qquad 3.22$$

and $\sigma_D(V) = 0$ if $V_c > V$

or $V_c < V + \frac{e}{C}$

$\sigma_D(V) = 1$ otherwise .

1 is chosen arbitrarily as any constant. But the limits for integration are zero and e/C.

For $0 < V$, if $V < \frac{e}{C}$,

$$\int_0^{e/C} \sigma_D(V_c)\, dV_c = \int_0^{V} dV_c = V$$

if $V > \frac{e}{C}$

$$\int_0^{e/C} \sigma_D(V_c)\, dV_c = \int_0^{e/C} dV_c = \frac{e}{C}$$

For $0 > V$, if $V > -\frac{e}{C}$

$$\int_0^{e/C} \sigma_D(V_c)\, dV_c = \int_{V-e/C}^{-e/C} dV_c = -V$$

if $V < -\frac{e}{C}$

$$\int_0^{e/C} \sigma_D(V_c)\, dV_c = \int_0^{e/C} dV_c = \frac{e}{C} \quad .$$

Putting these results in (3.22) gives

$$\langle\sigma(V)\rangle = \frac{C}{e}\,|V| \qquad \text{for} \quad |V| < \frac{e}{C} \qquad 3.23a$$

$$\langle\sigma(V)\rangle = \frac{C}{e} \cdot \frac{e}{C} = 1 = \text{constant} \qquad \text{for} \quad |V| > \frac{e}{C} \qquad 3.23b$$

The variation of $\langle\sigma(V)\rangle$ with voltage is shown in figure (3.6a).

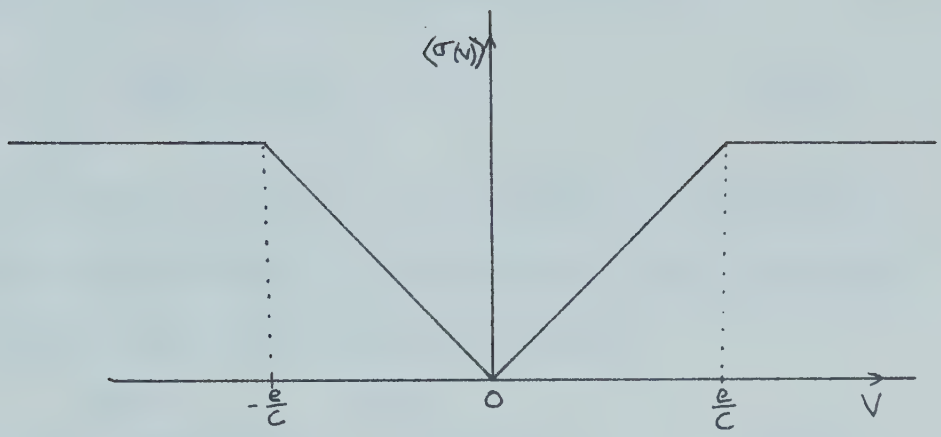

(a)

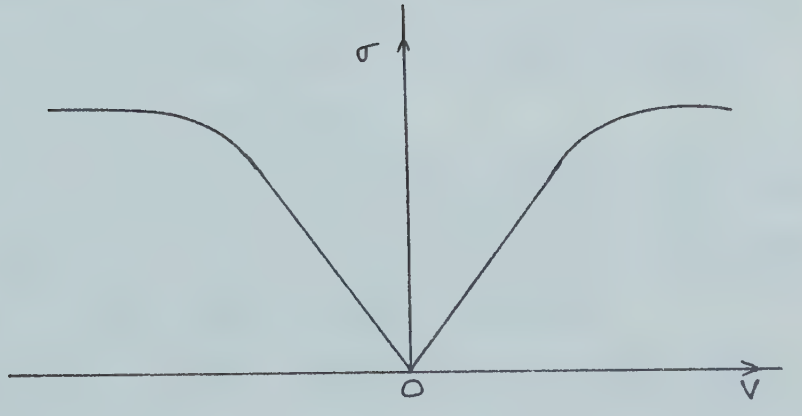

(b)

Figure 3.6
(a) The conductance of a set of particles with fixed capacitance C.
(b) The conductance of a number of particles f(C) with a distribution of capacitance C.

For a distribution of particles such that f(C) is the number of particles with capacitance C,

$$\sigma(V) \propto \int_0^\infty CdCf(C) \langle\sigma(V)\rangle \quad . \qquad 3.24$$

The factor C comes in since $\sigma(V)$ depends on the capacitance which in turn depends on the area of the capacitor plates. Using (3.23) and taking positive V,

$$\sigma(V) = \frac{V}{e} \int_0^{e/V} dC\, C^2 f(C) + \int_{e/V}^\infty CdCf(C) \quad . \qquad 3.25$$

The number of particles f(C) is determined by the distribution of particles. The conductivity given by equation 3.25 is illustrated in figure (3.6b). $\sigma(V)$ increases linearly for small applied bias voltages and the main contribution comes from the large particles since for these $C^2 f(C)$ is maximum.

Townsend et al (1971) have discussed the case for non-zero temperatures. Their derivation gives the first term of equation (3.25) temperature dependent.

For particles of given capacitance C, the number F(C) of excited particles is proportional to $\exp(-eV_c/kT)$ and the number of particles of capacitance C with activation energy between V_c and V_c+dV_c is $\frac{C}{e} f(C)dV_c$. Thus

$$F(C) = \frac{C}{e} f(C)dV_c \exp(-\frac{eV_c}{KT}) \quad .$$

The contribution to the conductivity is

$$\frac{C^2}{e} f(C)dC\ e^{-eV_c/kT}$$

$$\sigma(V_c,T) = \int_0^\infty \frac{C^2}{e} f(C)\ dC \int_0^\infty e^{-eV_c/kT}\ dV_c$$

$$= \frac{k}{e^2} \int_0^\infty C^2 f(C)\ dCT \qquad 3.26$$

at $V_c = 0$,

$$\sigma(0,T) \propto T \ .$$

The second term which appears in (3.25) is left out in (3.26). It becomes important at voltages greater than e/C.

When the particles become superconducting, the activation energy increases by half the energy gap; eV_c becomes $eV_c + \Delta$. Equation (3.19) has to be replaced by the normal metal-superconductor voltage dependence. These changes will cause $(dI/dV)_{V=0}$ to fall and this will be reflected in the conductivity as the critical temperature is reached.

CHAPTER 4

EXPERIMENTAL PROCEDURES

A. Sample Preparation

A tunnel junction is simply a metal-insulator-metal sandwich , henceforth referred to as M_1-I-M_2, deposited on a suitable substrate such as a glass microscope slide. Such junctions with particles deposited in the insulator, referred to as M_1-M_3^P-M_2, were fabricated.

A glass microscope slide was cleaned with a detergent under running tap water, dried with optical wiper tissue and then passed over a hot flame to remove impurities by ionization bombardment.

In the case where M_1 and M_2 were tin, indium metal contacts were made on the glass microscope slide before mounting in the slide holder. If contacts were made after evaporation of tin, the tin film was found to break due to the low melting point of tin.

Evaporation techniques in the preparation of thin films and particles have been discussed by Holland (1967) and Chopra (1969). After attaining a vacuum of about 10^{-6} torr in the evaporating-bell-jar system, M_1 was deposited and the surface oxidised as described in the following section. M_3 particles of different

sizes controlled by the quartz crystal thickness monitor were deposited and then the surface was allowed to oxidise slightly. Finally M_2 was deposited to complete the junction. The stages are shown in figure 4.1.

I) Oxidation

Different methods of oxidation were tried.

(i) Aluminium

Aluminium oxidises easily even at room temperature. Aluminium oxide of desired resistance was formed by glow discharge under 0.1 torr of oxygen and a total current of 1 mA. By allowing longer times of current flow, oxides of higher resistances could be obtained. With the aluminium film 4.5 cm from the aluminium electrode, 8 minutes duration gave a tunnel resistance of about 200 Ω. Miles and Smith (1963) have given a good account of this method.

Thermal oxidation in air under humid conditions and in dry oxygen at one atmosphere were also tried. In the latter case the glass microscope slide was held over a heated semi-cylindrical copper sheet. The temperature was recorded by a thermocouple. Again by fixing the heating current and hence the temperature, the duration time was the major factor determining the resistance of the oxide.

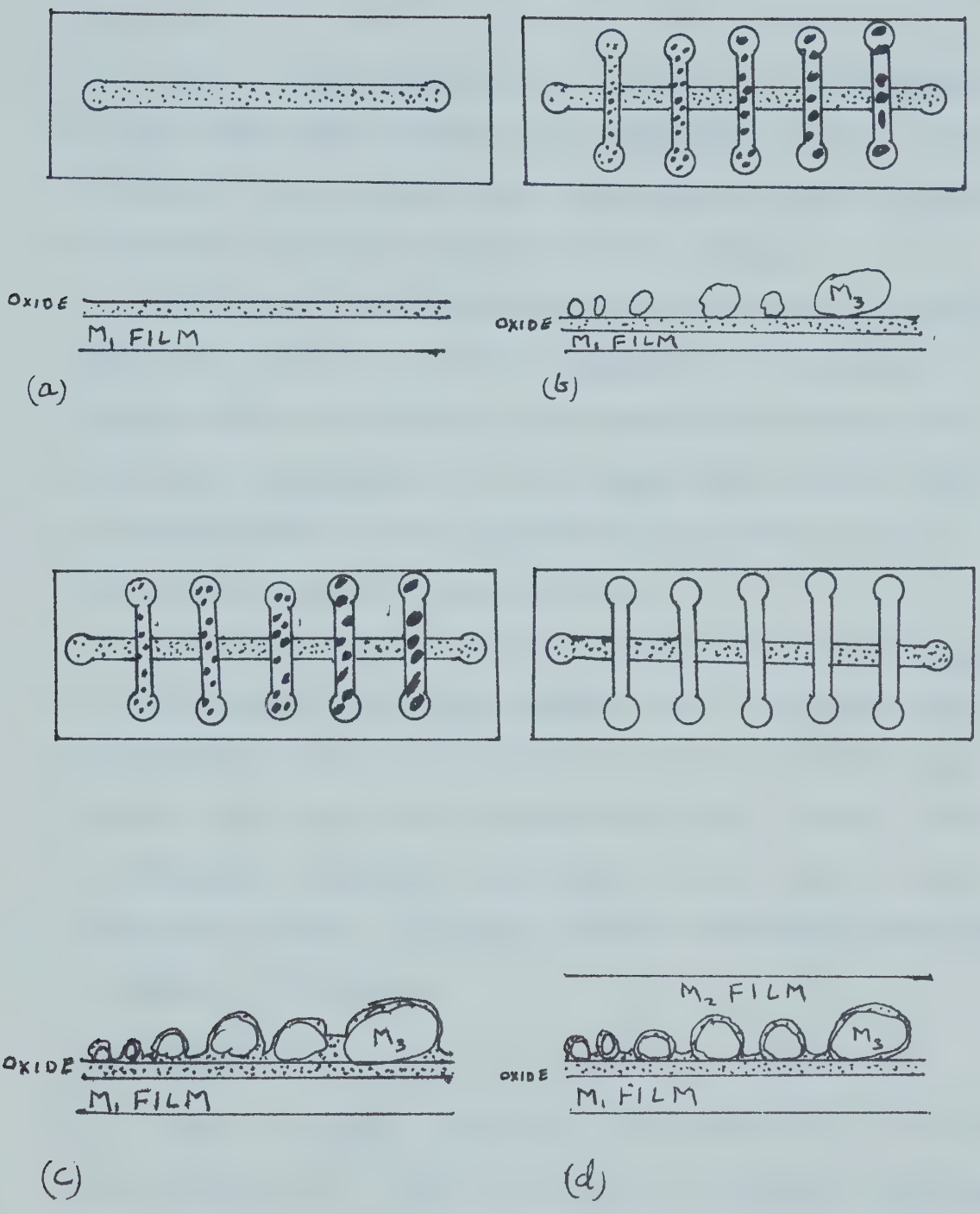

Figure 4.1

Sample preparation stages

(a) Slightly oxidised M_1 film

(b) M_3 particles on top of the oxide of M_1

(c) The surface of the particles lightly oxidised

(d) Final film of M_2 counter electrode.

(ii) Tin

Tin is more difficult to oxidise. Good barriers of tin oxide were obtained by evaporating tin at a rate of about 4 Å per second and oxidising the film surface by thermal oxidation for two to four hours.

Tin forms continuous films at relatively thicker films and the film structure depends on a number of things such as the nature and temperature of the substrate, the temperature of the evaporating source, rate of evaporation and the residual gas pressure in the evaporating system, Chopra (1969).

At high rates of evaporation, tin molecules impinge on the substrate in large numbers, and nucleation and coalscence of the grains proceed rapidly forming large islands and then a milky continuous film. Such a film is difficult to oxidise, Walmsley (1965). But at low evaporation rates, no milky film is formed and the film is easier to oxidise.

(iii) Lead

Lead is easily oxidised in an atmosphere of oxygen. With aluminium as a base electrode, the tunnel resistance is much larger but it does not increase with time as in the case of Aluminium-Aluminium oxide-Tin. This observation agrees with Handy's (1962) results.

Oxides of lead were formed by exposing lead films to one atmosphere of dry oxygen for 5-20 minutes. In the case of lead particles, the resistance of the tunnel junction increased rapidly with increasing thickness of the lead particles. It is suggested that with the low melting point of lead, for small particles a number of them have the oxide over them breaking down on evaporating the final electrode, aluminium, which has a much higher boiling point. As a result the resistance is reduced for very small particles and one gets a situation with Al-I-Al, Al-I-Pb-I-Al and Al-I(Pb)Al altogether forming the tunnel junction. This suggestion is supported by the results of junctions with small particles of lead.

II) Deposition of Particles

In the film formation process, after nucleation, the grains coalesce into small particles which then amalgamate to form a continuous film. The idea is to get amounts of evaporated metal M_3 without reaching the continuous film formation stage.

After a constant rate of evaporation of metal M_3 was attained, particles were deposited onto the oxide. The rate was about 10 Å per second in the case of tin particles and about 20 Å per second in the case of lead.

The amount evaporated was controlled using a quartz crystal thickness monitor described in section B. The size and distribution of particles of lead was observed with the electron microscope, plates 5.1 and 5.2.

The surfaces of the particles were oxidised to form a thin oxide. In the case of tin, thermal oxidation was for about two hours while for lead a few minutes in dry oxygen gave a reasonable oxide thickness.

Particles for observing in the electron microscope were deposited on an oxidised Al base held on the electron microscope grid by surface tension, simultaneously with the junctions. The electron micrographs were analysed as described in section B of Chapter 5.

B. Thickness Measurement

The thickness of an evaporated film was monitored during evaporation by a quartz crystal thickness monitor.

Two 5 MHz crystals mounted in the same water cooled holder, figure (4.2c), one exposed to the evaporating sample and the other in thermal contact with the copper holder for heat compensation during evaporation were connected to the quartz crystal monitor as shown in figure (4.2b).

This kind of thickness monitoring device utilizes the principle that the resonance frequency of a piezo-

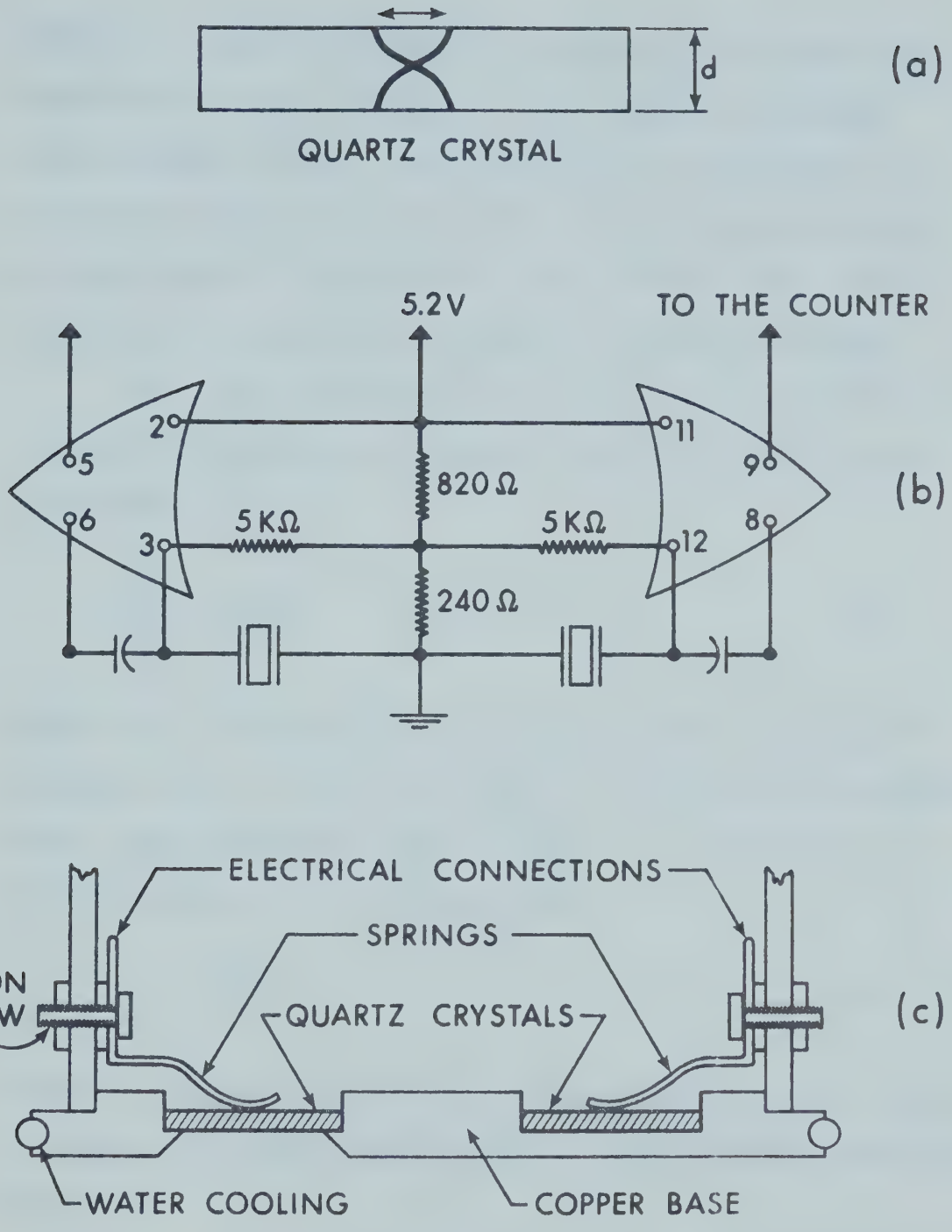

Figure 4.2

A Quartz Crystal Thickness Monitor

(a) The oscillation of a single crystal; most of the mass displacement occurs at the crystal surface.
(b) The circuit diagram of the crystal monitor used in this work. The integrated circuit is a Motorola MC 1024 P.
(c) Crystal holder; very light springs are used to provide electrical contacts with the crystals.

electric crystal depends on the mass of the material deposited on the surfaces of the crystal, Eschbach and Kruidhof (1965). The oscillation frequency is a decreasing function of the mass of the film deposited on the crystal and changes quite linearly with film thickness as long as the crystal is not overloaded.

The rate of deposition is found by observing the change in frequency Δf, which is proportional to the mass added, Δm

$$\frac{\Delta f}{f_o} = \frac{\Delta m}{m} \qquad 4.1$$

where m is the mass of the quartz crystal of natural frequency f_o. When the crystal is excited to thickness-shear oscillations, figure (4.2a), f_o is related to the thickness, d, by the equation

$$f_o = \frac{C_\perp}{2d} \qquad 4.2$$

where $C_\perp$ is the transverse velocity equal to the velocity of sound in quartz (3340 m/sec). The frequency shift is given by

$$\Delta f = -\frac{C_\perp}{2d^2}\Delta d = -\frac{2f_o^2}{C_\perp}\Delta d$$

$$\frac{\Delta f}{f_o} = \frac{2f_o}{C_\perp}\Delta d = \frac{2f_o}{C_\perp}\frac{\Delta m}{\rho_q A} \qquad 4.3$$

where ρ_q is the density of a quartz crystal with area A and Δm is the change in mass. If Δm is the added mass of the evaporating material with density ρ,

$$\Delta f = \frac{2f_o^2}{C_\perp} \frac{\rho t}{\rho_q}$$

where t is the thickness of the evaporated material

$$t = \frac{C_\perp \rho_q}{2f_o^2 \rho} \Delta f \quad . \qquad 4.4$$

The crystal can be lightly damped at its periphery without disturbing its mode of oscillation appreciably. Warner and Stockbridge (1963) found that this description of the crystal monitor is accurate within 1%. Hartman (1965) found the density of thin films to be less than that of the bulk sample.

In our case, experimental arrangements are such that particles from the evaporating sample strike the crystal at an angle θ with the vertical, so that there is a factor of $\cos^3\theta$ in the constant $2f_o^2\rho/C_\perp\rho_q$. For small angles $\cos\theta \sim 1$. Since the film density is somewhat variable, the constant is best determined experimentally using the crystal measurements together with the Tolansky interferometer measurements. Vrba (1971) has described these measurements in detail. The values used in this work are shown in table (4.1). In all thickness measurements, t will refer to average thickness.

Table 4.1

Material	ρ(bulk) gm/cm^3	$\frac{2f_o^2\rho}{C_1\rho_q}$ ppm/KÅ
Al	2.70	220
Sn	5.75	440
Pb	11.34	850

C. Production of Low Temperature

The experimental arrangement for the production of low temperature is shown in figure (4.3). In the figure, (P) is the pumping chamber provided with a needle valve (a) to allow in the chamber the desired amount of liquid nitrogen or liquid helium. A stainless steel tube (b) provided with thermal shield (h) connects (P) to a rotary pump. By pumping over liquid helium, a temperature of about 1°K could be reached. A regulating pressure valve to control the pressure above the helium allows a variation of temperature between 1°K and 4.2°K. Elevated temperatures up to 70°K could be maintained using an electronic controller which senses the resistance of a 220 Ω speer carbon resistor (d). (s) is the sample chamber which contains the sample holder (e) and the germanium thermometer (g). The vacuum chamber (V) is connected to a diffusion pump and a pressure of 1×10^{-6} torr is needed to shield the sample from the liquid helium bath (t) which is surrounded by liquid

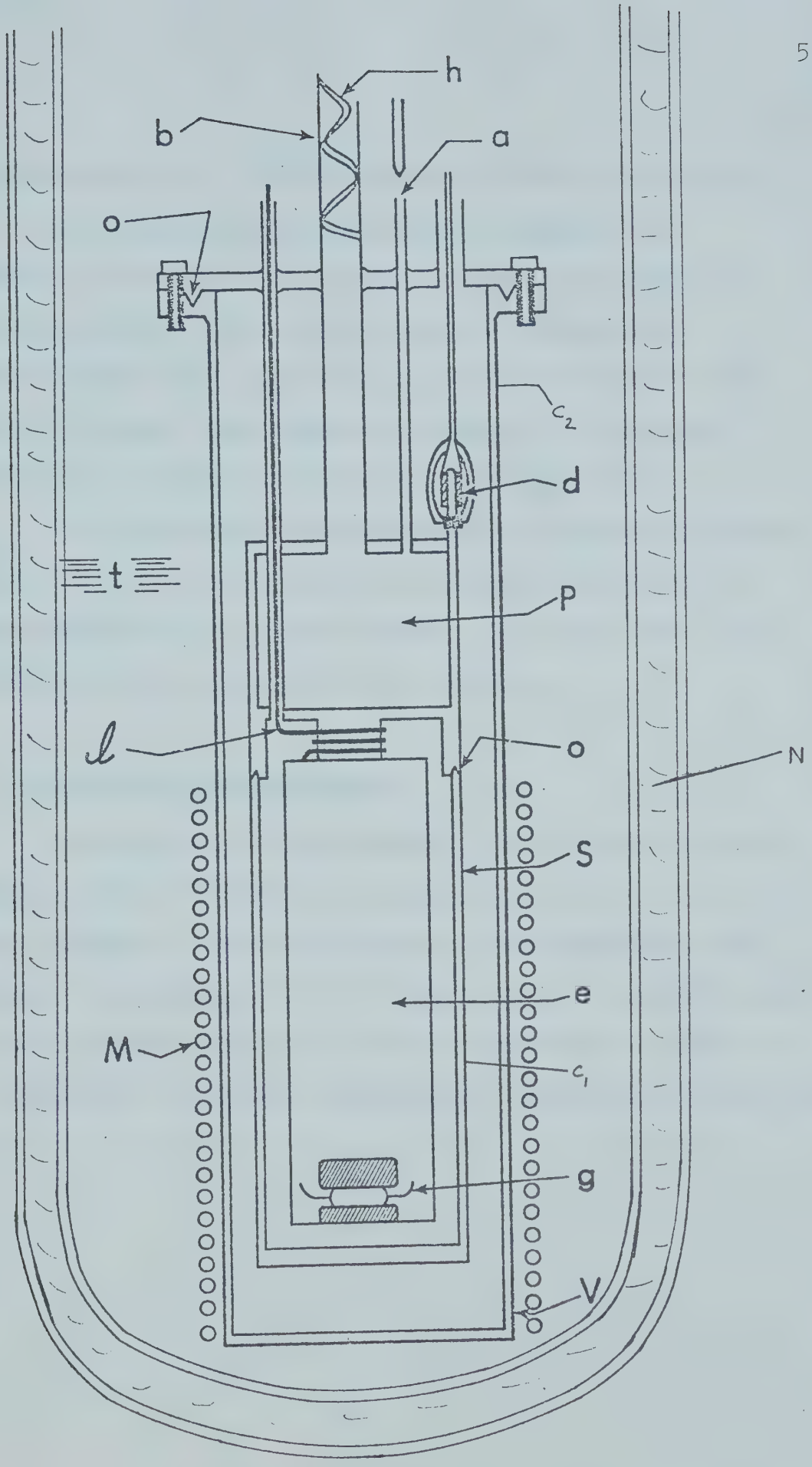

Figure 4.3
The cryostat arrangement for the production of low temperature.

nitrogen bath (N). The cryostat was designed to fit in a bore of a 20 KG superconducting magnet (M). Indium 0 rings (0) plus apiezon grease were used for vacuum sealing. The grease makes it possible to separate the cans (c_1) and (c_2) without damaging the indium 0 rings, thus making it possible to use the seals four or five times before repairing them.

For temperature measurements the germanium thermometer #904 was calibrated by Dr. Rogers between 1°K and 60°K and by Dr. Woods between 4.2°K and 12°K. The bridge used was designed by Dr. Rogers.

D. Conductance Measurements

The dynamical conductance $\sigma = di/dV$ and its derivative $d\sigma/dV = d^2i/dV^2$ are measured as functions of the bias voltage V. The conductance bridge used for this purpose was designed by Dr. Rogers and has been described by him, Rogers (1970). A lock in amplifier is used as the detector and an X-Y plotter for recording the results.

CHAPTER 5

EXPERIMENTAL RESULTS AND DISCUSSION

A. Tin Particles

(i) Sn-Sn^P-Sn Junctions

A conductance dip at zero bias is observed even at room temperature but more pronounced at 80°K and below. Of the three junctions shown in figure(5.1), the one with average particle thickness of 50 Å has the greatest dip.

In figure (5.2) the dip is very large. At low voltages the conductance-voltage dependence is linear but rolls off at higher voltages. The general shape of the curves is similar to that predicted by the capacitor model, figure (3.6).

At low temperatures when Sn is superconducting, figure (5.3), a peak at 1.15 mV and a step at about 2.5 mV are observed. The peak decreases as the particle size increases implying that direct tunneling between the films is not important for large size particles. The position of this peak determines the energy gap of Sn where $V = 2\Delta_{Sn}$. Tunneling between the films becomes important as the particle size becomes smaller. This is so since the activation energy for smaller particles is higher.

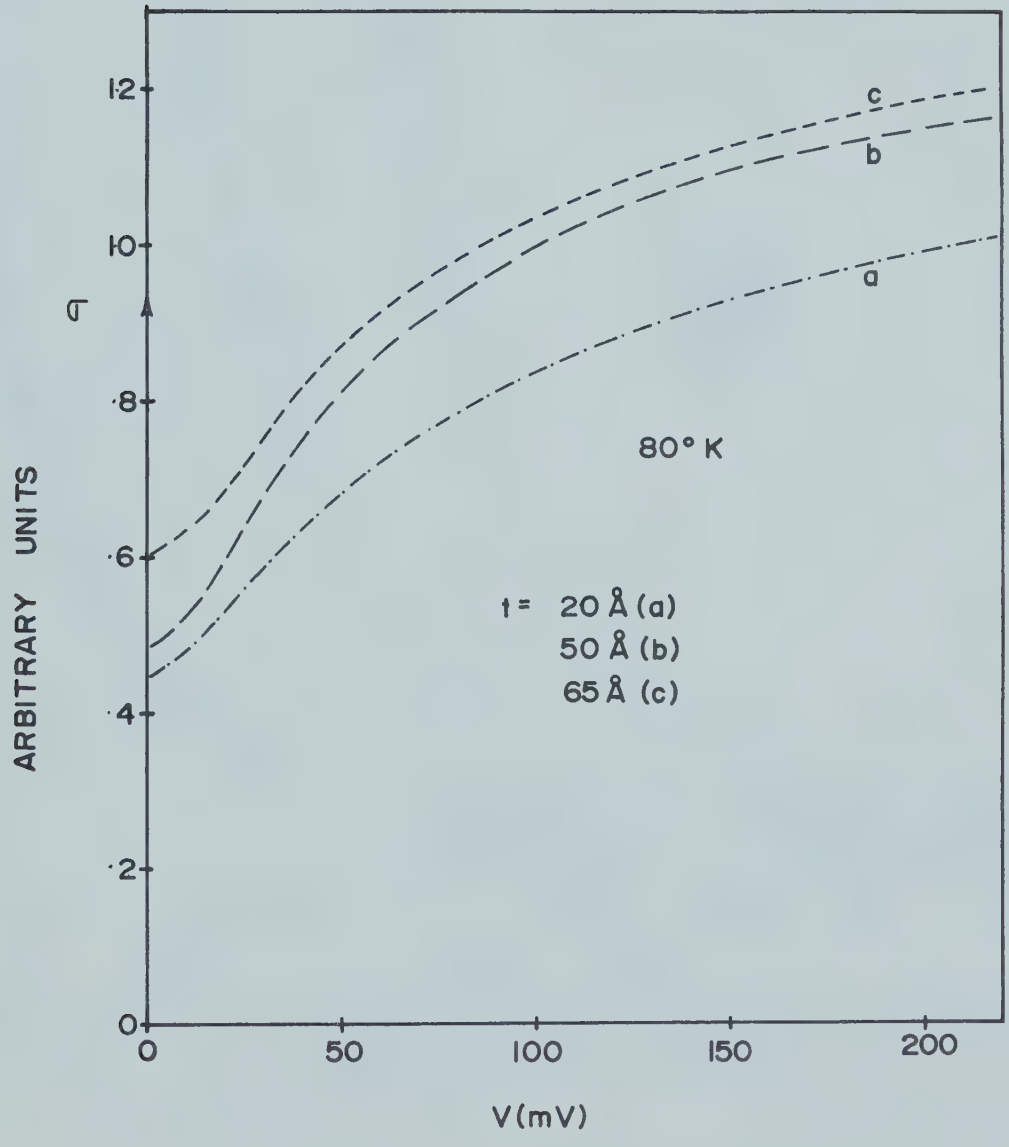

Figure 5.1. Voltage dependence of the conductance σ of three different junctions of Sn-Sn^{P}-Sn at 80°K.

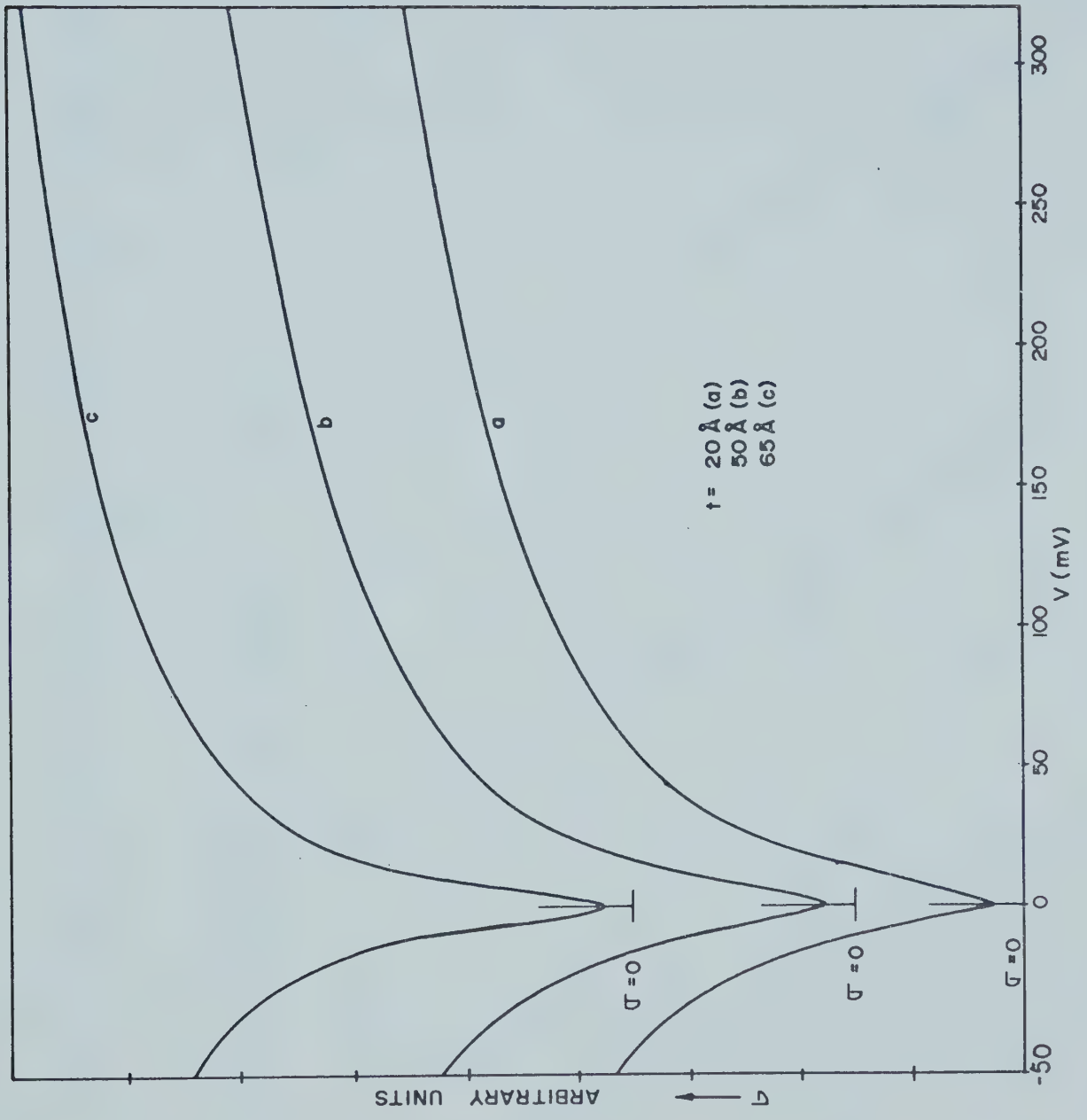

Figure 5.2. Voltage dependence of the conductance σ of three different junctions of Sn-Sn^{P}-Sn at 4.2°K.

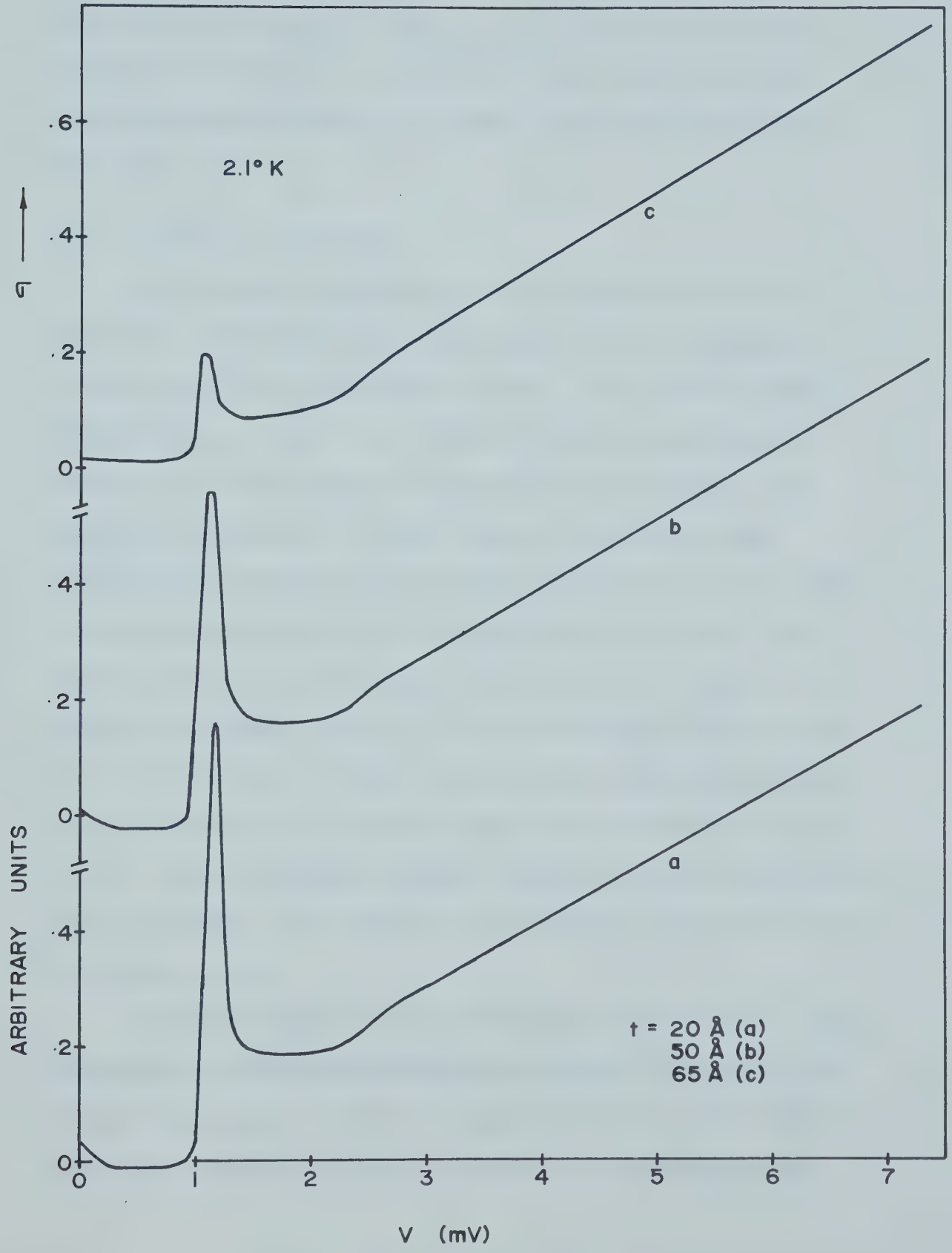

Figure 5.3. The conductance versus voltage for three different junctions of Sn-Sn^P-Sn at 2.1°K.

The step occurs at about 2.5 mV and this is equivalent to $2\Delta_{film} + 2\Delta_{particles}$, similar to two junctions in series. In section B we shall see that the second derivative of i gives a more precise point for this step.

(ii) Al-Sn^P-Al Junctions

The voltage dependence of the conductance for Al-Sn^P-Al junctions shown in figure (5.4) is similar to the Sn-Sn^P-Sn junctions at 80°K. At liquid helium temperatures, figure 5.5, the zero bias conductance anomaly is also similar except that the rolling off occurs in a smaller voltage range. For small bias voltages the conductance is linear rolling off at higher voltages depending on the average particle size. For large particles, for example curve (e) (t = 130 Å), it levels off almost sharply. The conductance dip at zero bias, $\sigma(0)$, varies almost linearly for small particles. This is shown on the bottom right hand corner of figure (5.5). The half-width becomes narrower as the particle size increases. The shape of the curves agrees with that of figure (3.6).

At lower temperatures, shown in figure (5.6), when aluminium is superconducting, the energy gap cannot be noticed implying no direct tunneling between the films. The step at about 1.4 mV can hardly be distinguished.

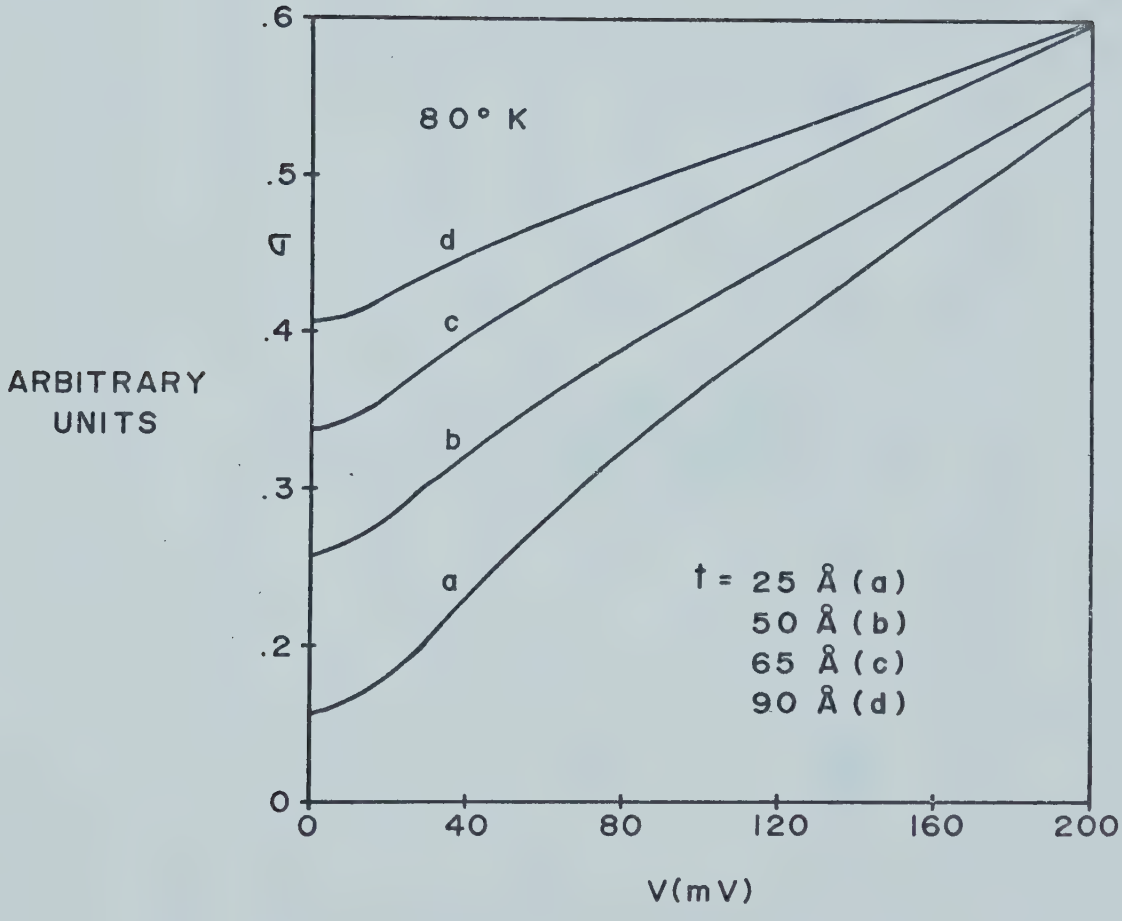

Figure 5.4. Voltage dependence of the conductance σ of four different junctions of Al-Sn^{P}-Al at 80°K.

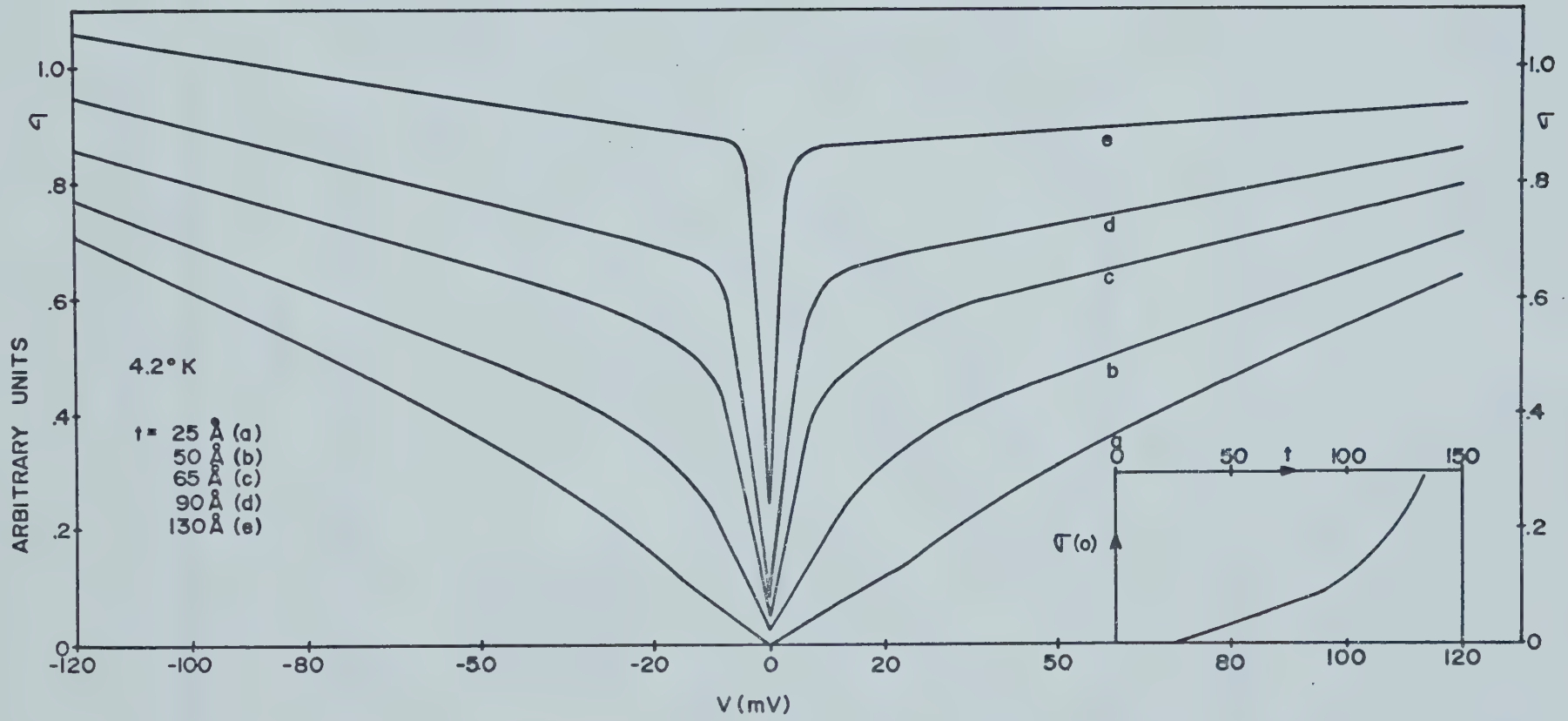

Figure 5.5. Voltage dependence of the conductance σ of five different junctions of Al-Sn^{P}-Al at 4.2°K and the particle size dependence of σ(0).

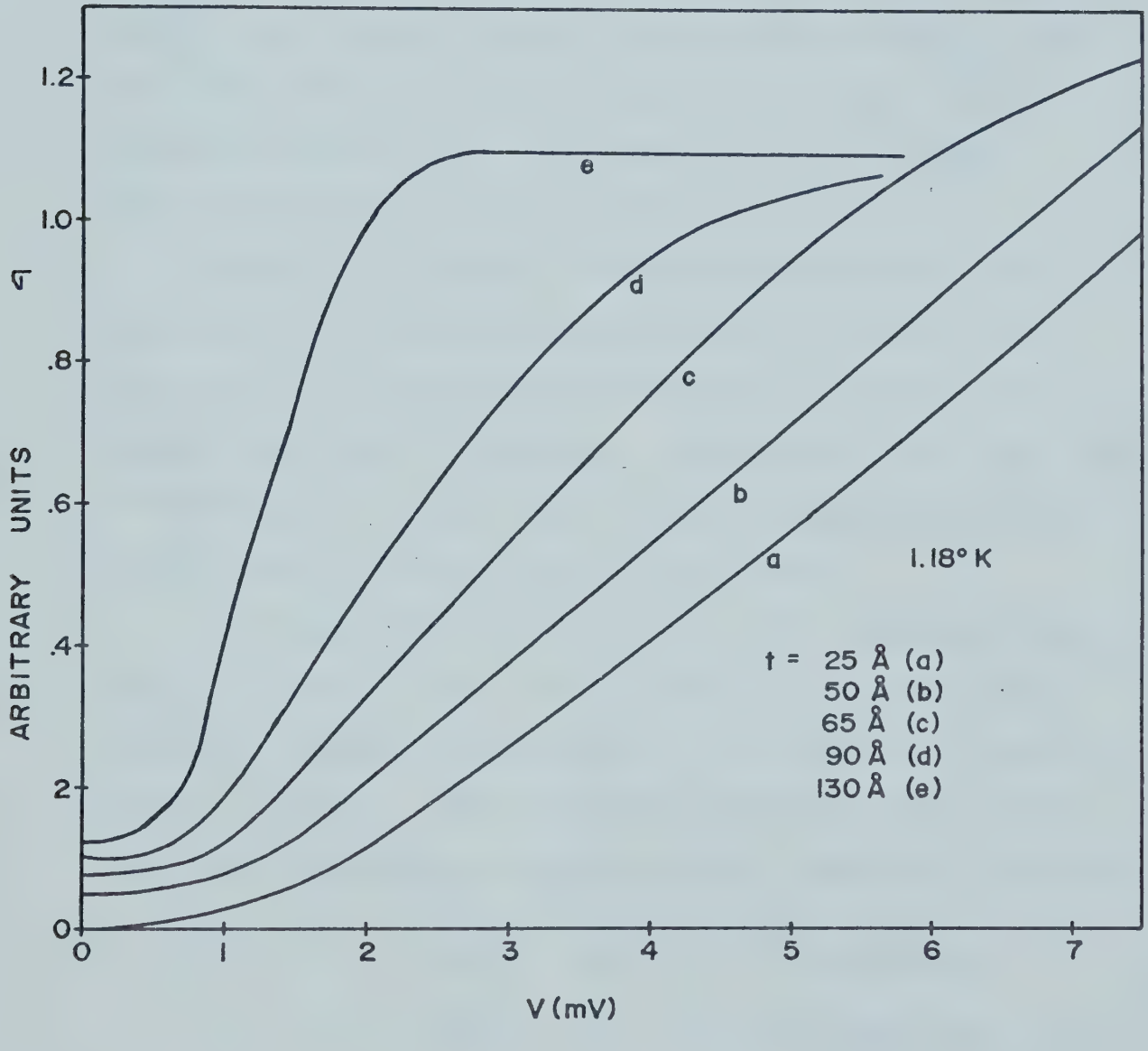

Figure 5.6. Conductance-voltage characteristics of five different junctions of Al-Sn^{P}-Al at 1.2°K.

The voltage at which the conductance saturates depends on the particle size as can be seen in curves (e) and (d). With very thick particles, shown in figure 5.7, two junctions in series behaviour becomes prominent. The first peak at 0.8 mV is equivalent to $(\Delta_{Al} + \Delta_{Sn})$ and the next one at 1.27 mV is equivalent to $2\Delta_{Sn}$ and the third one at 1.9 mV corresponds to $(2\Delta_{Al} + 2\Delta_{Sn})$. one would suspect this last peak to reach a maximum when the particles form a continuous film.

Figure (5.8) shows the conductance-voltage characteristics for different applied magnetic fields. The curve at zero field is displaced when a field of reasonable magnitude is applied. The maximum field that could be applied due to the superconducting magnet was 20 KG and we could not reach the critical field.

The temperature dependence of the conductance is shown in figure (5.9). It is linear for temperatures above the critical temperature T_c of Sn and this confirms equation (3.26). When Sn particles become superconducting, the conductance decreases moving away from linearity.

$T_c = 4.15 \pm 0.05°K$ for t = 65Å particles

$T_c = 4.05 \pm 0.05°K$ for t = 130Å particles

$T_c = 3.72°K$ for bulk Sn (Lynton(1962)).

When the linear curve is extrapolated, the $\sigma(0)$ intercept gives the background conductance of 27%, 4% and 14% for particles of average thickness 65Å, 90Å and 130Å respectively.

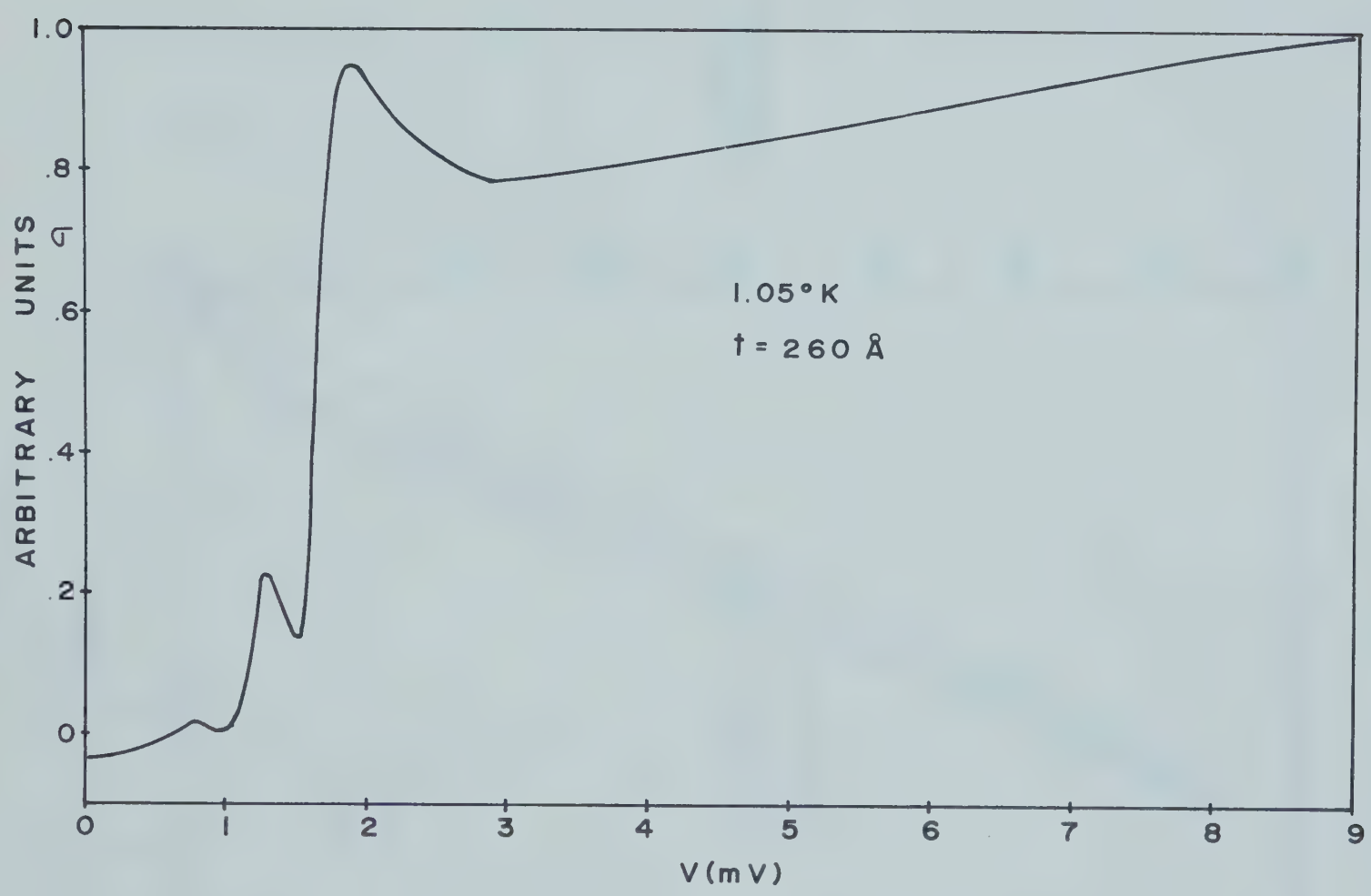

Figure 5.7

Two junctions in series-like behaviour for very thick particles.

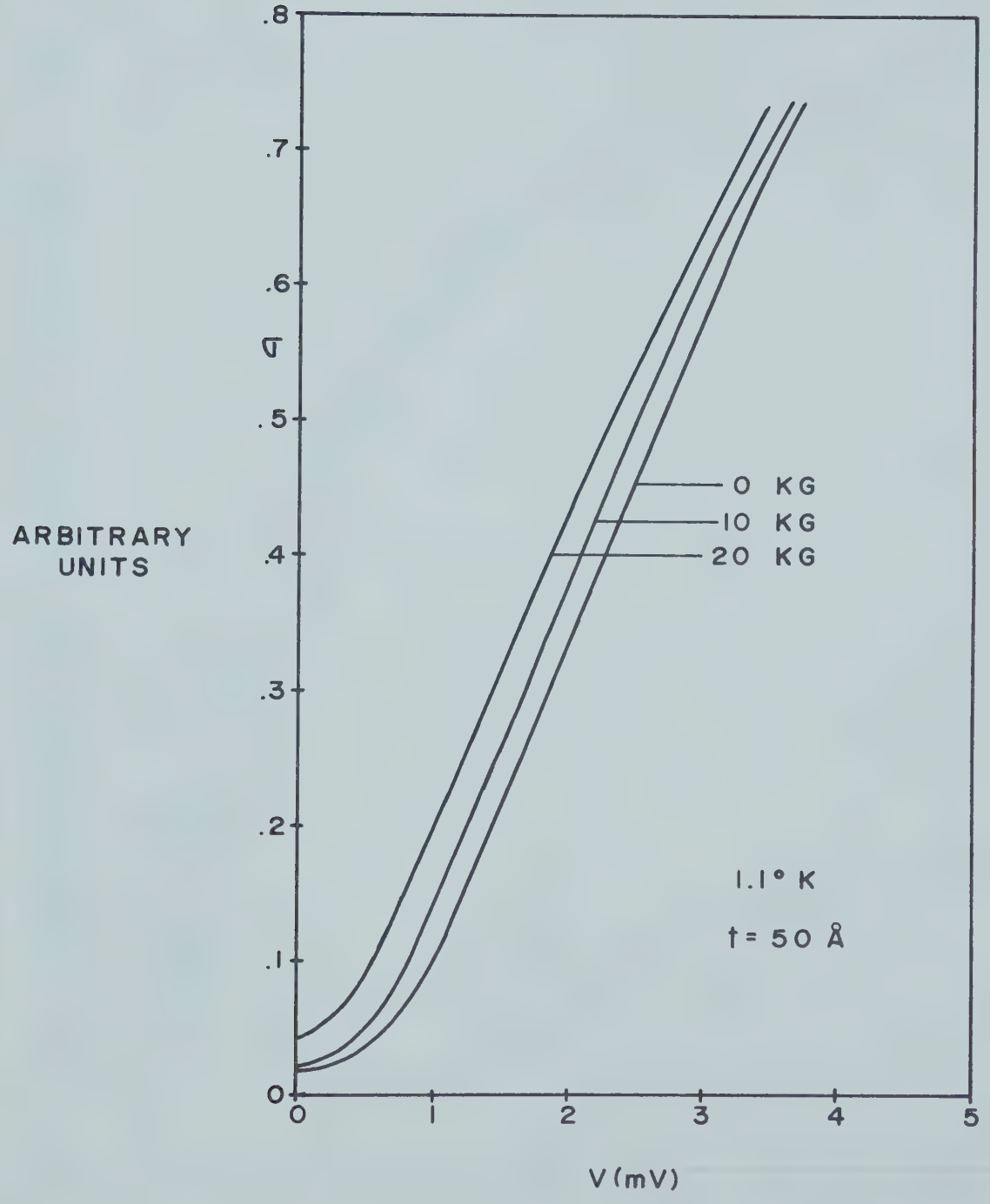

Figure 5.8

The magnetic field effect on the conductance-voltage characteristic.

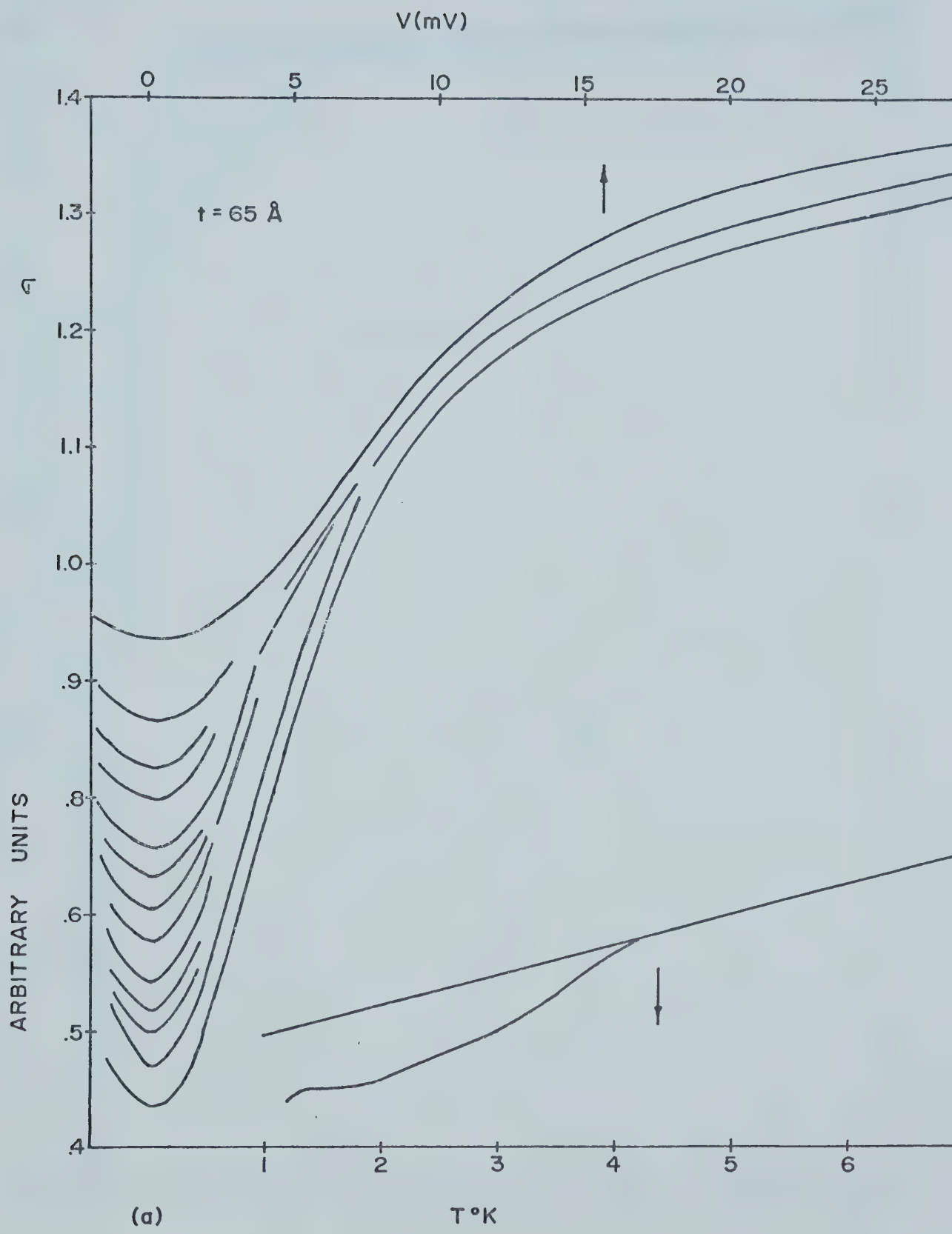

Figure 5.9(a). The temperature dependence of the conductance σ; average particle thickness, t=65 Å.

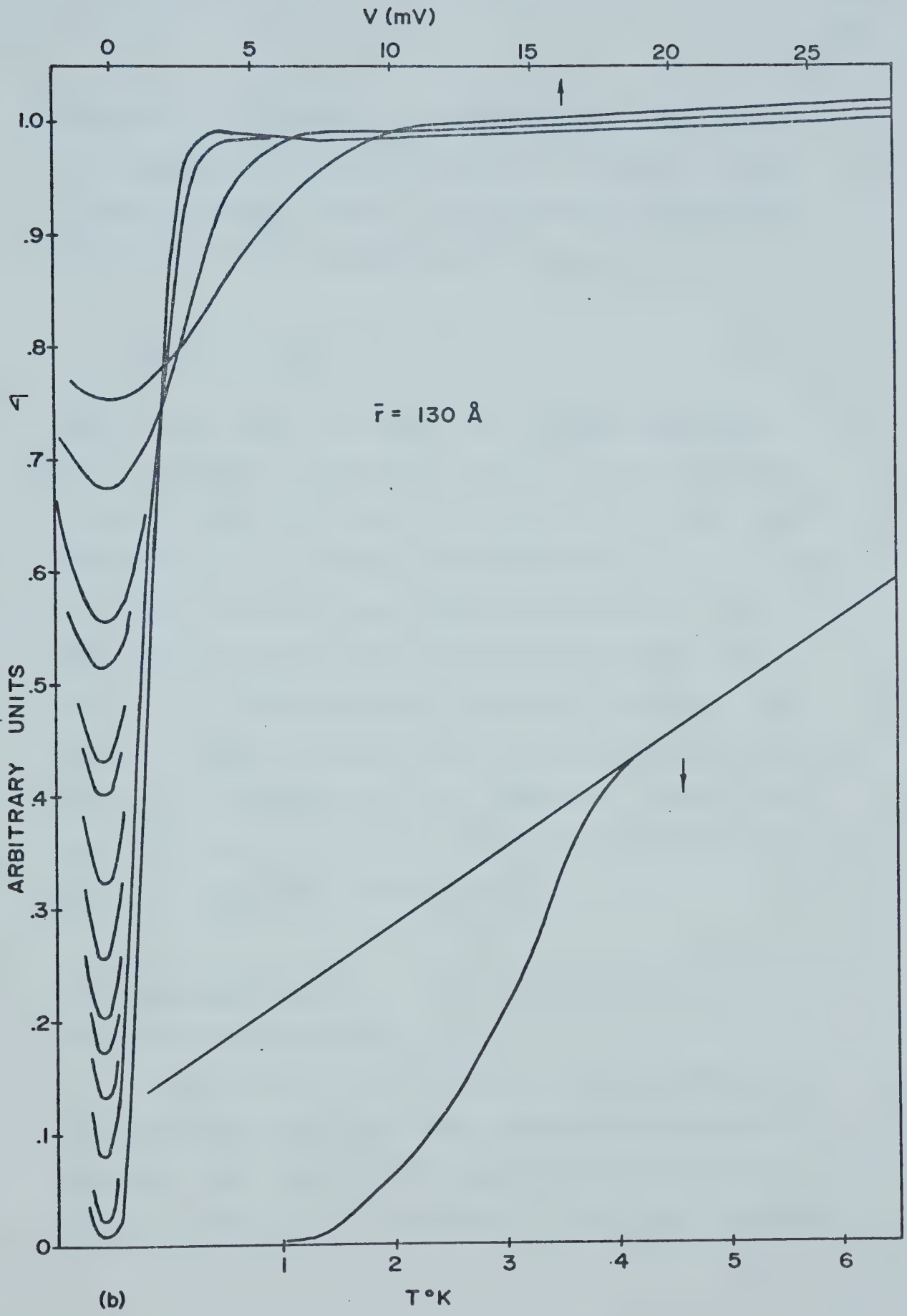

Figure 5.9(b). The temperature dependence of the conductance σ; average particle thickness, t=130 Å.

According to Blumberg and Seraphin (1963) the transition temperature of metals such as In and Al, and Sn in some respects, whose T_c increases with decreasing thickness T_c is connected by the relation

$$T_\Delta = \frac{A}{t} - \frac{B}{t^2} \qquad 5.1$$

where A and B are constants and t is the thickness. Our T_c results at least show that T_c for Sn particles is higher than the value for bulk Sn. The temperature dependence of the normalised conductance σ_s/σ_n is shown in figure 5.10 for three different junctions. For the 90 Å curve $T_c = 4.5 \pm .1°K$ and one would expect this curve to lie between the 65 Å and 130 Å curves. This does not happen because according to Giaever's suggestion there is a maximum size effect somewhere between 50 Å and 100 Å for Sn particles. Below 50 Å and above 100 Å particle sizes the effects fade out.

B. Lead Particles

(i) Particle Distribution

Particles and thin films are usually prepared by the condensation of atoms from the vapour phase of the material. The way in which particles and thin films come into being can be ascribed to this growth process.

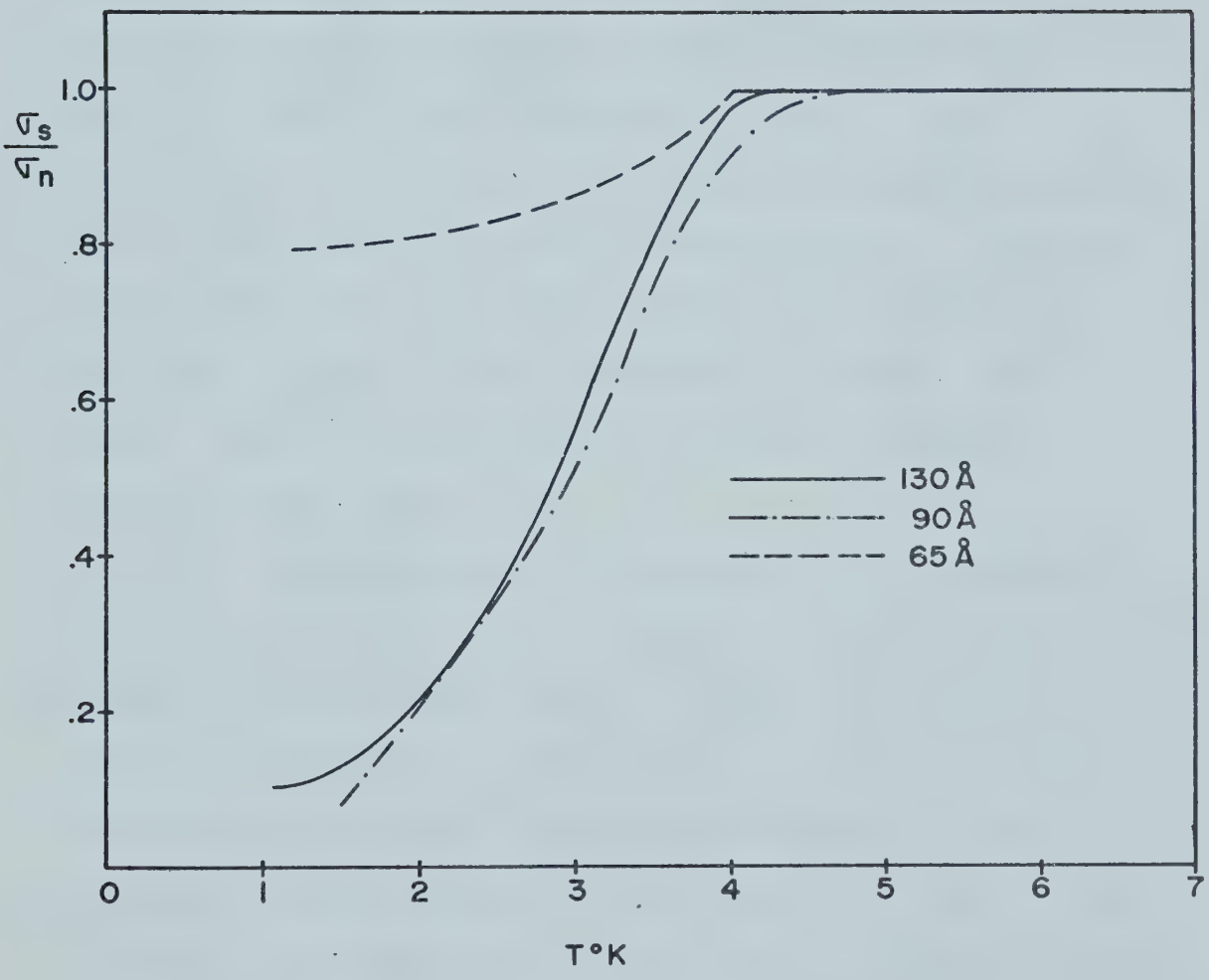

Figure 5.10. The temperature dependence of the normalized conductance σ_s/σ_n.

Nucleation is the birth stage. It is a problem of vapour-solid-phase transformation. Pocza (1967) has discussed a number of parameters influencing the structure formation. Such parameters are M, the nature of the material evaporated characterised by purity, chemical reaction, etc.; V, the vapour beam which would be atomic or molecular, characterised by temperature, pressure and evaporation rate; P, the residual gas pressure; S, the substrate characteristics; and W, the evaporation source characterised by geometry, temperature, etc. All these parameters interact with each other making it very difficult to survey them. Chopra (1969) has discussed in detail the formation stages of thin films.

The impinging atom is attracted to the substrate surface by the instantaneous dipole and quadrupole moments of the surface atoms. It loses its normal velocity provided the kinetic energy is not too large. Thus the vapour atom is physically absorbed, it may not be thermally equilibrated, it may move over the surface by jumping from one potential well to the other implying that the absorbed atom has a finite "stay" time on the surface during which it may interact with other atoms. Alternatively the vapour atom could bounce off especially if its kinetic energy is very high. The probability

that an impinging atom will be incorporated into the substrate is called the "condensation" or "sticking" coefficient α_T

$$\alpha_T = \frac{T_I - T_R}{T_I - T_S} = \frac{E_I - E_R}{E_I - E_S} \qquad 5.2$$

where the T's and E's are the root mean square temperatures and kinetic energies of the incident (I), reflected (R) and substrate (S) respectively.

For two different surfaces, say Al_2O_3 on an electron microscope grid and Al metal on a quartz crystal, which receive equal numbers of vapour atoms, the distributions of the condensed particles may be different or one surface might have more vapour atoms reflected than the other. We assume that the distribution of particles observed in the electron microscope is the same as that in the junctions prepared simultaneously. Plate (5.1a) shows an electron micrograph of Pb particles on Al_2O_3. The average thickness of such particles is 180 Å measured by the quartz crystal thickness monitor. Plate (5.1b) shows the diffraction pattern. There is a high probability that particle distribution may not be uniform even within the same junction. Plate (5.2b) shows this. In plate (5.2a) the large dark spots in the background are assumed to be due to the detergent used in the

Plate 5.1

(a) Electron micrograph of lead particles of average thickness 180 Å.

(b) The diffraction pattern of particles in (a).

Plate 5.2

Electron micrographs of lead particles of average thickness

(a) 60 Å

(b) 130 Å

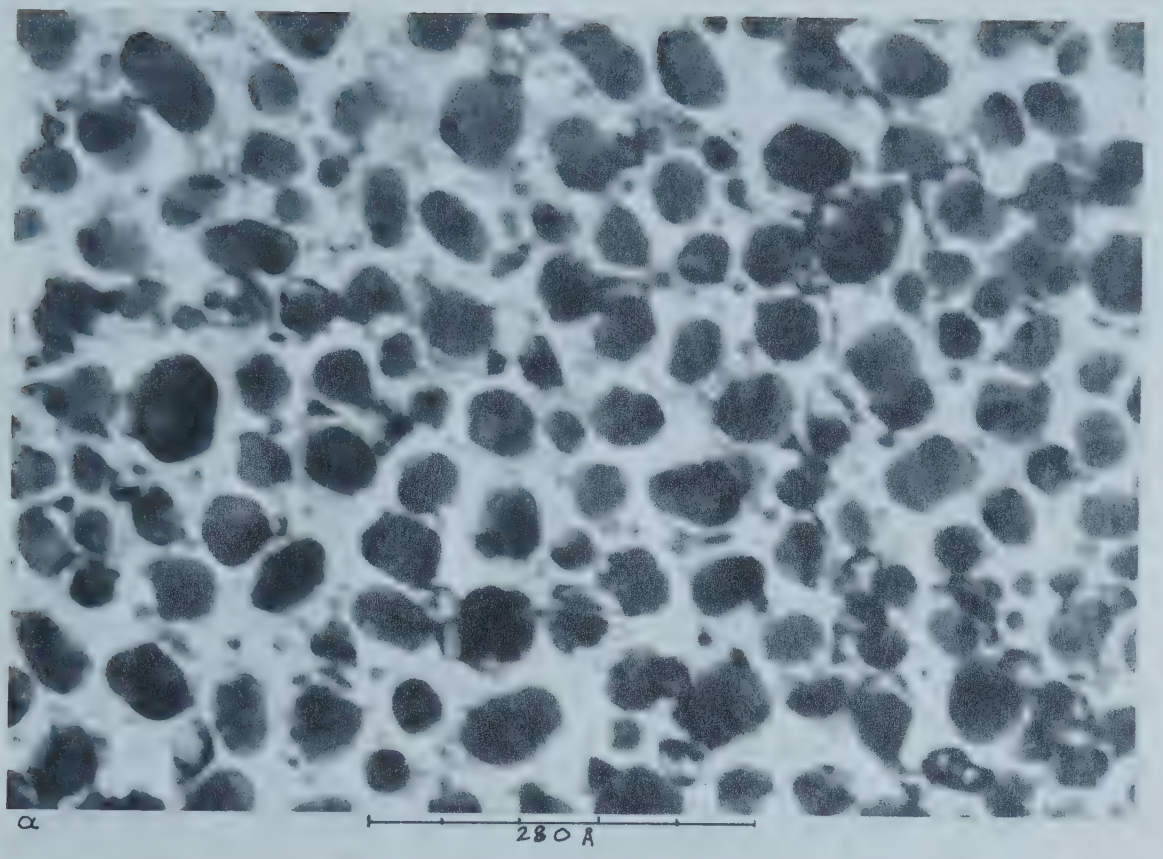

a

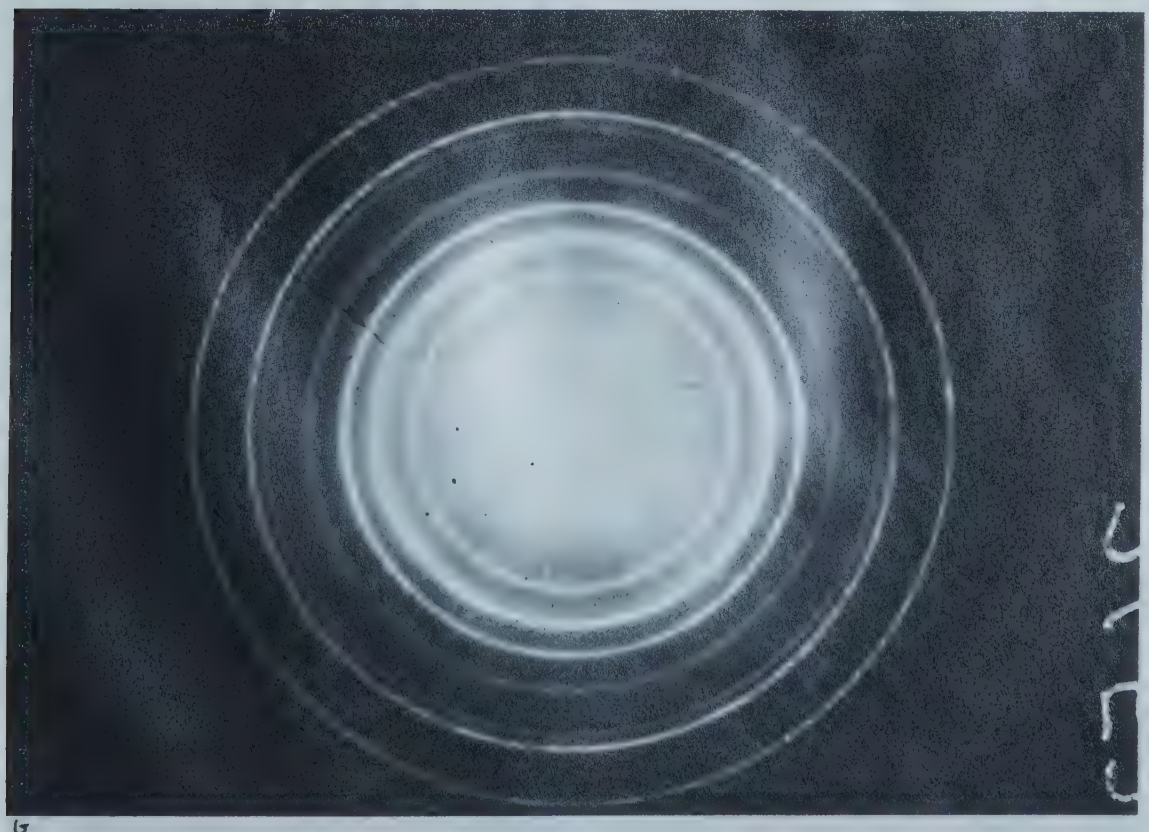

b

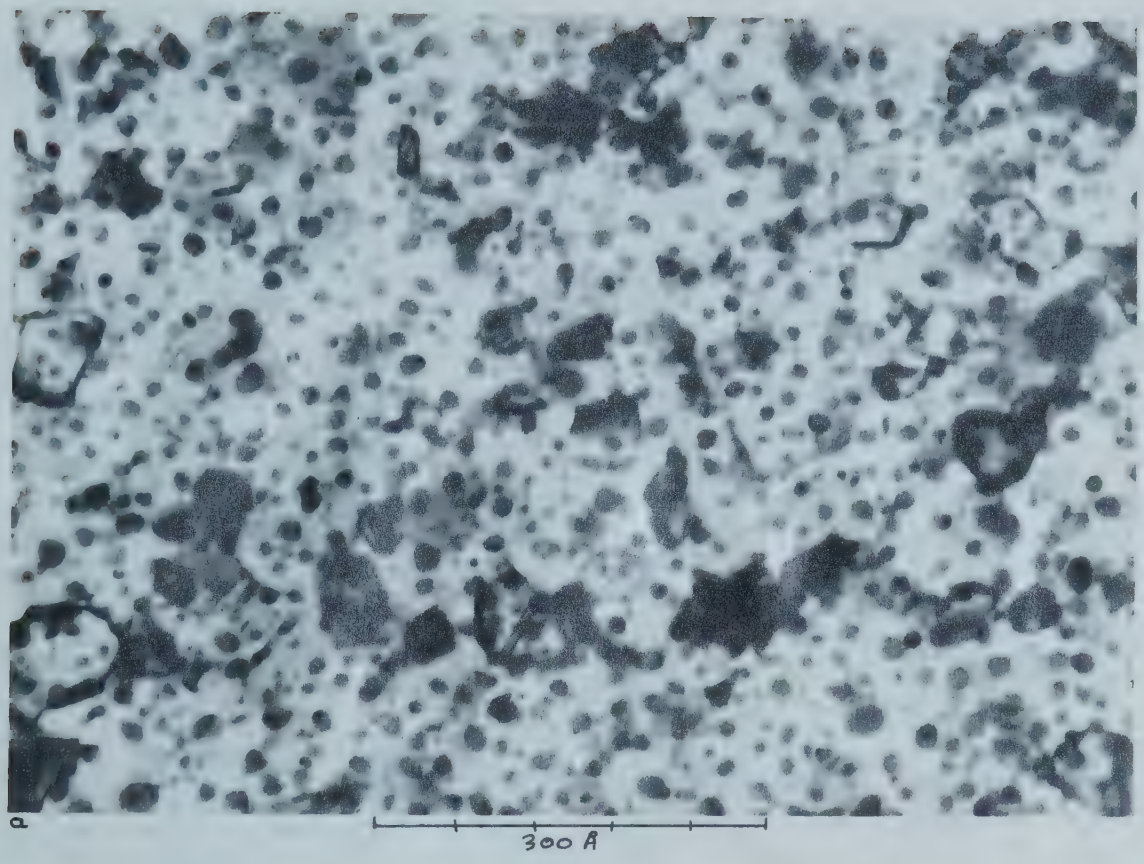
a
300 A

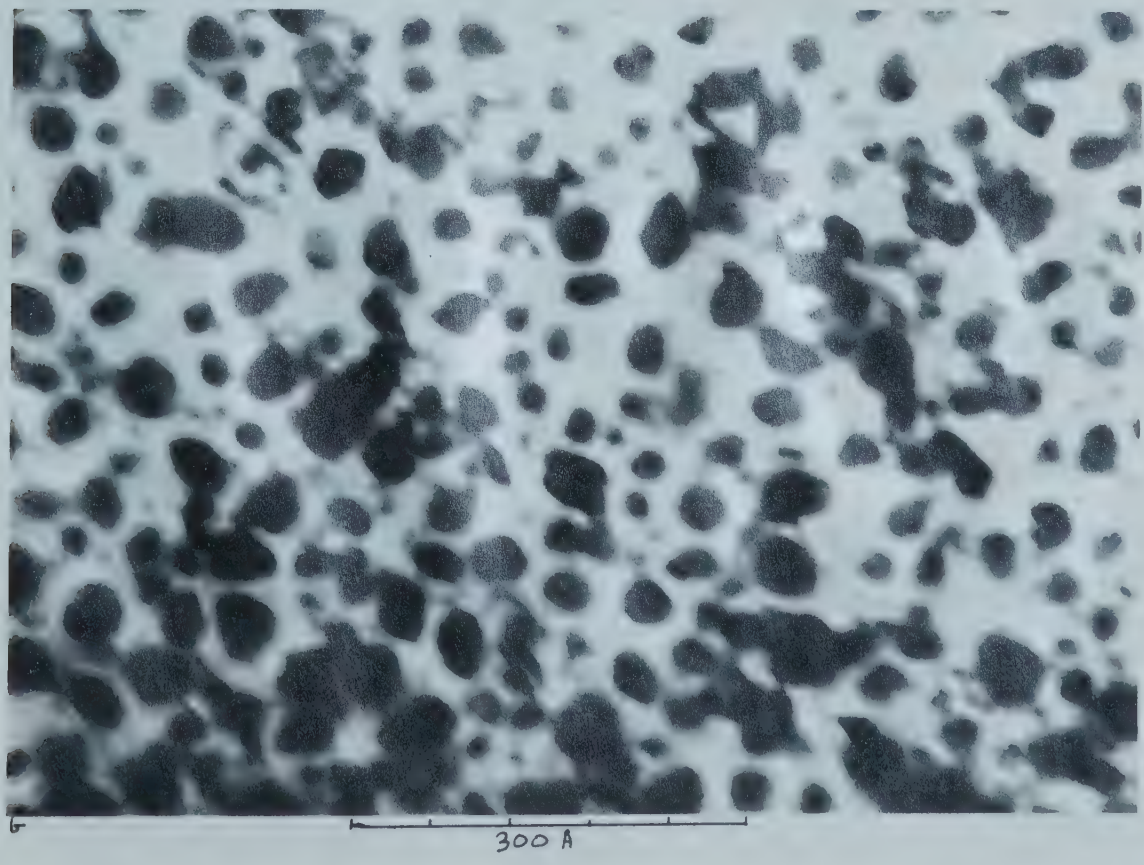
b
300 A

preparation of the base for the electron microscope grid.

Particle distribution functions have been derived by Chakraverty (1967) and Basset et al (1959). The functions are of statistical nature. The electron micrograph of plate (5.2a) was enlarged ten times and areas of the visible particles measured giving a histogram shown in figure (5.11). The dotted curve of figure (5.11) was approximated to the curve of the function

$$P(v^2) = \frac{\Gamma(7)}{\Gamma(5)\Gamma(2)} 10^5 4^2 \frac{(v^2)^4}{(4 + 10v^2)^7} \qquad 5.3$$

for the v^2 distribution with 10 and 4 degrees of freedom. Equation (5.3) was substituted in equation (3.25) for f(C) and numerically worked out on the computer. Figure (5.12) shows the curve plotted from the calculations. By adjusting the units, the measured conductance at 8°K and the calculated conductance are compared in figure (5.13).

From the mean area measurements, if we assume the particles approximately spherical, the average diameter was 110 Å compared to the average thickness of 60 Å measured by the quartz crystal thickness monitor. The ratio of total area of particles to total area of electron micrograph was 13%.

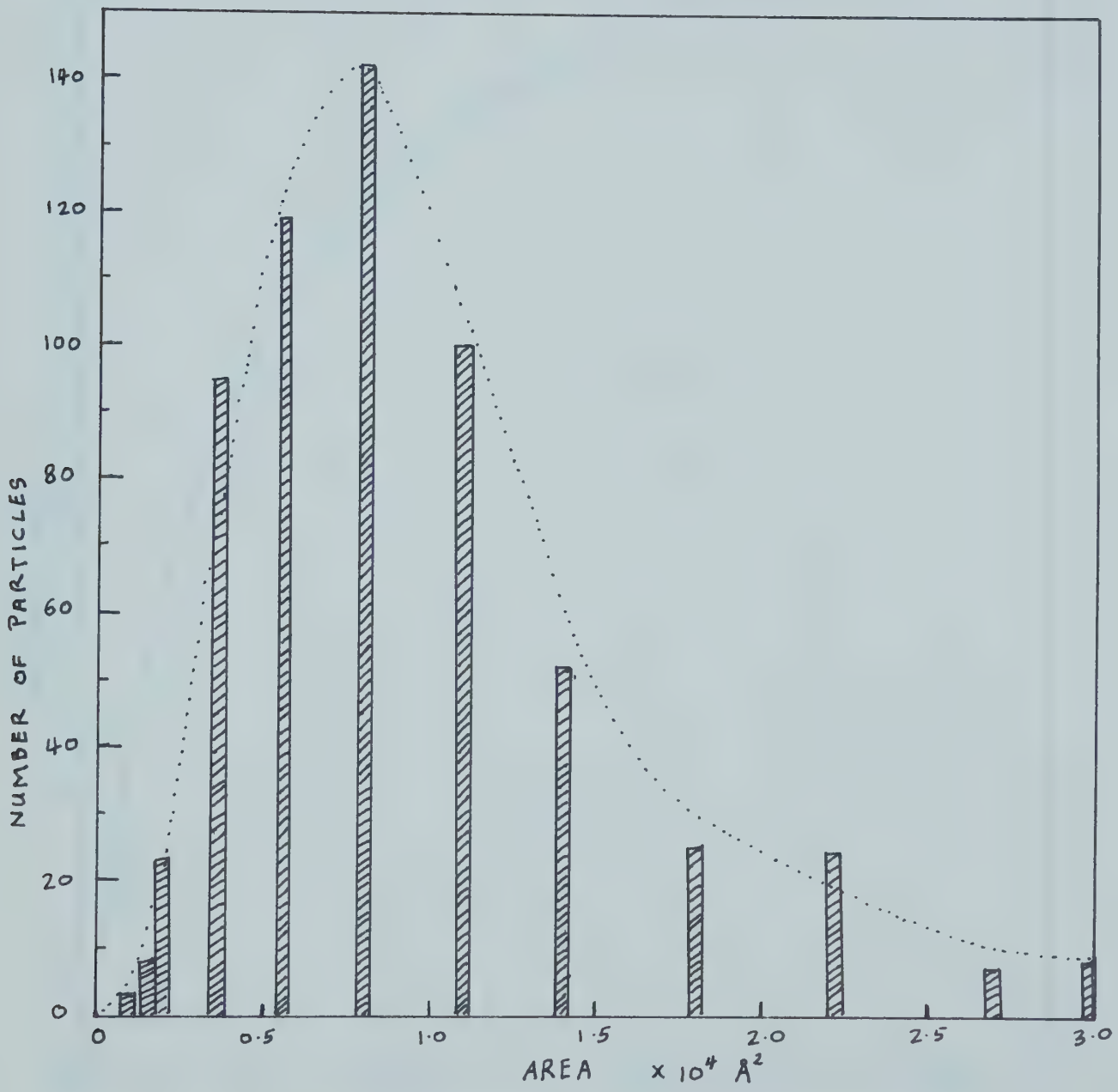

Figure 5.11. Particle distribution histogram for particles of thickness 60 Å.

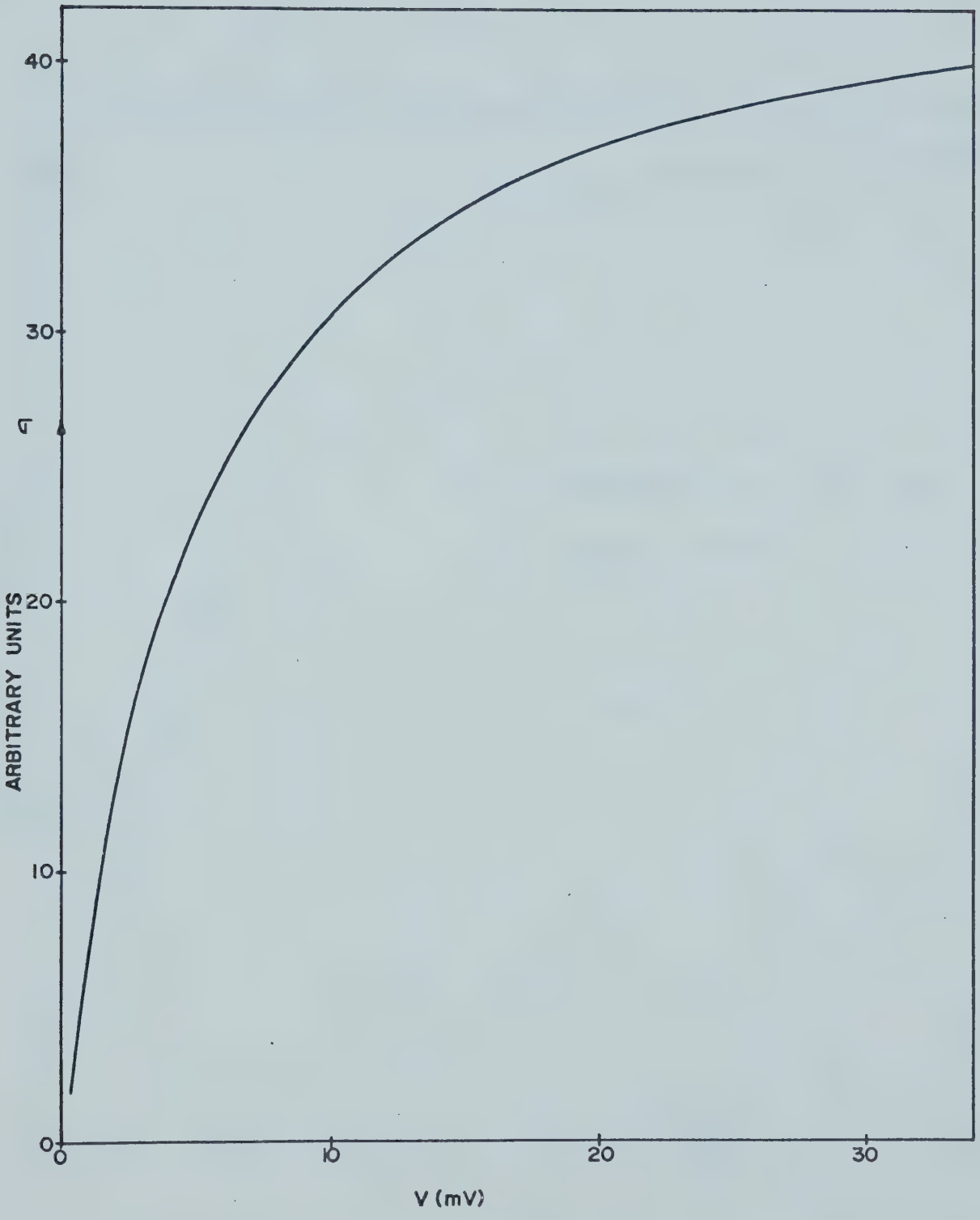

Figure 5.12. Computer curve for $\sigma(V)$ versus voltage characteristic for Pb particles of average thickness 60 Å.

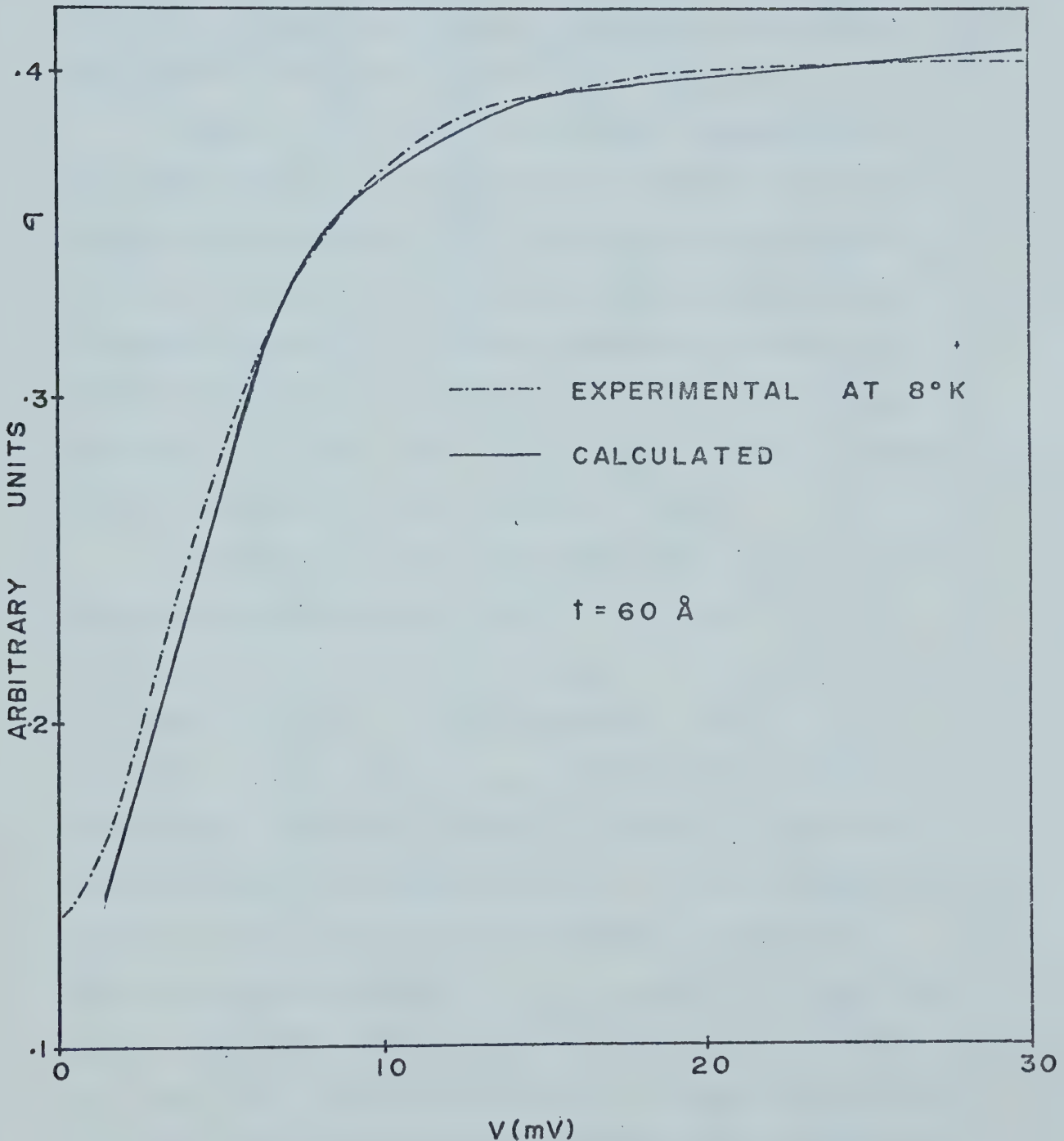

Figure 5.13. Measured (++ line) and calculated (solid line) conductance of a set of particles in the normal state, for particles of average thickness 60 Å.

(ii) Al-Pb^{P}-Al Junctions

In contact with Al_2O_3, lead formed increasingly high resistance junctions with increasing lead thickness even after a few minutes exposure in dry oxygen. This made it difficult to get good junctions.

Figure (5.14) shows the voltage dependence of the conductance of five different junctions at 8.1°K. Particles as small as 20 Å thick have no noticeable effect. The particle effect increases rapidly with increasing particle thickness reaching a maximum particle size effect and then decreases with increasing particle thickness. The shape of the curves is similar to that predicted by the capacitor model.

In figure 5.15 the four junctions show very interesting differences at 1.18°K. In curve (a) the first peak is at 0.35 mV equivalent to $2\Delta_{Al}$ and there is a small peak at 1.45 mV equivalent to $\Delta_{Al} + \Delta_{Pb}$. In curve (b) the peak at Δ_{Al} is diminished implying that direct tunneling between Al films is unimportant with increasing particle thickness. There is an extra peak at 1.16 mV which does not appear in curve (a). This peak is equivalent to $\Delta_{Pb} - \Delta_{Al}$ and the third peak in the same position as peak two in curve (a). These last two peaks suggest that there is tunneling between Al and Pb particles without localising the electrons on

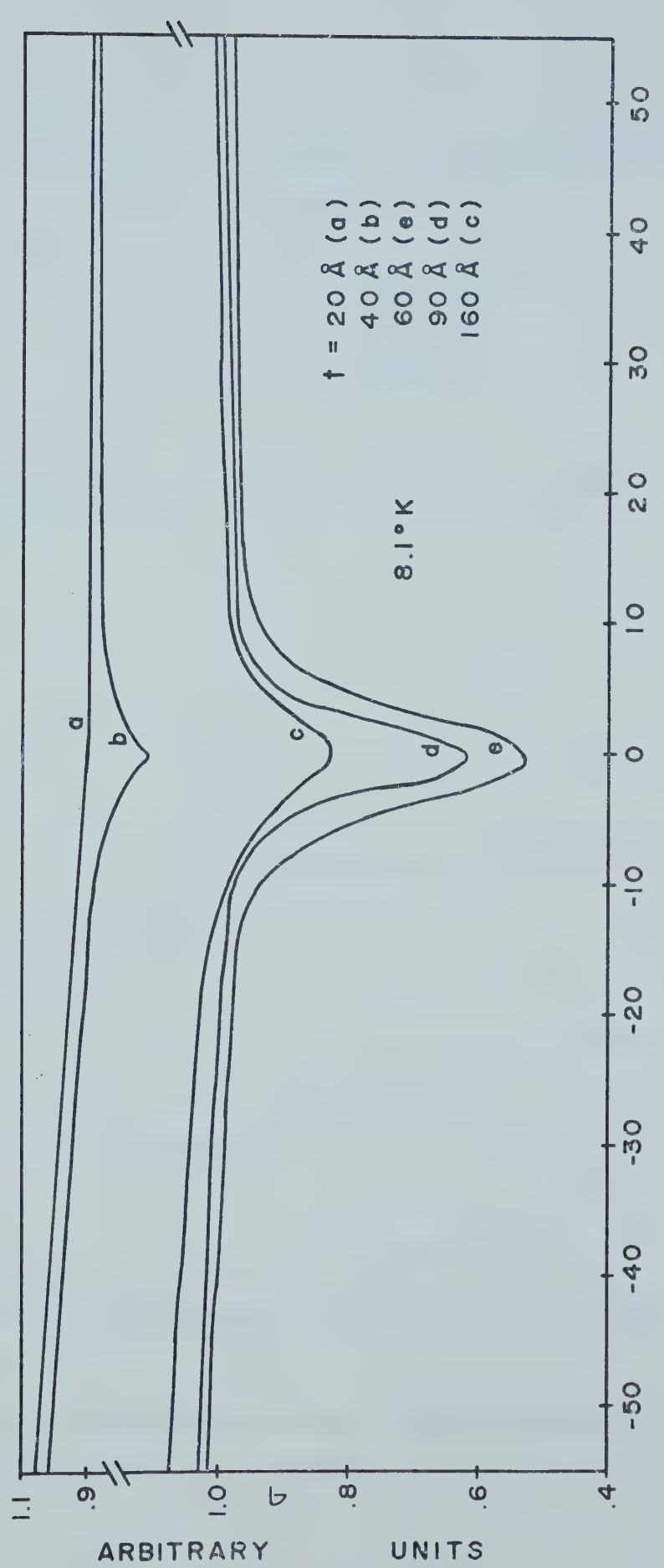

Figure 5.14. The voltage dependence of the conductance of different junctions of Al-Pb^{P}-Al at 8.1°K.

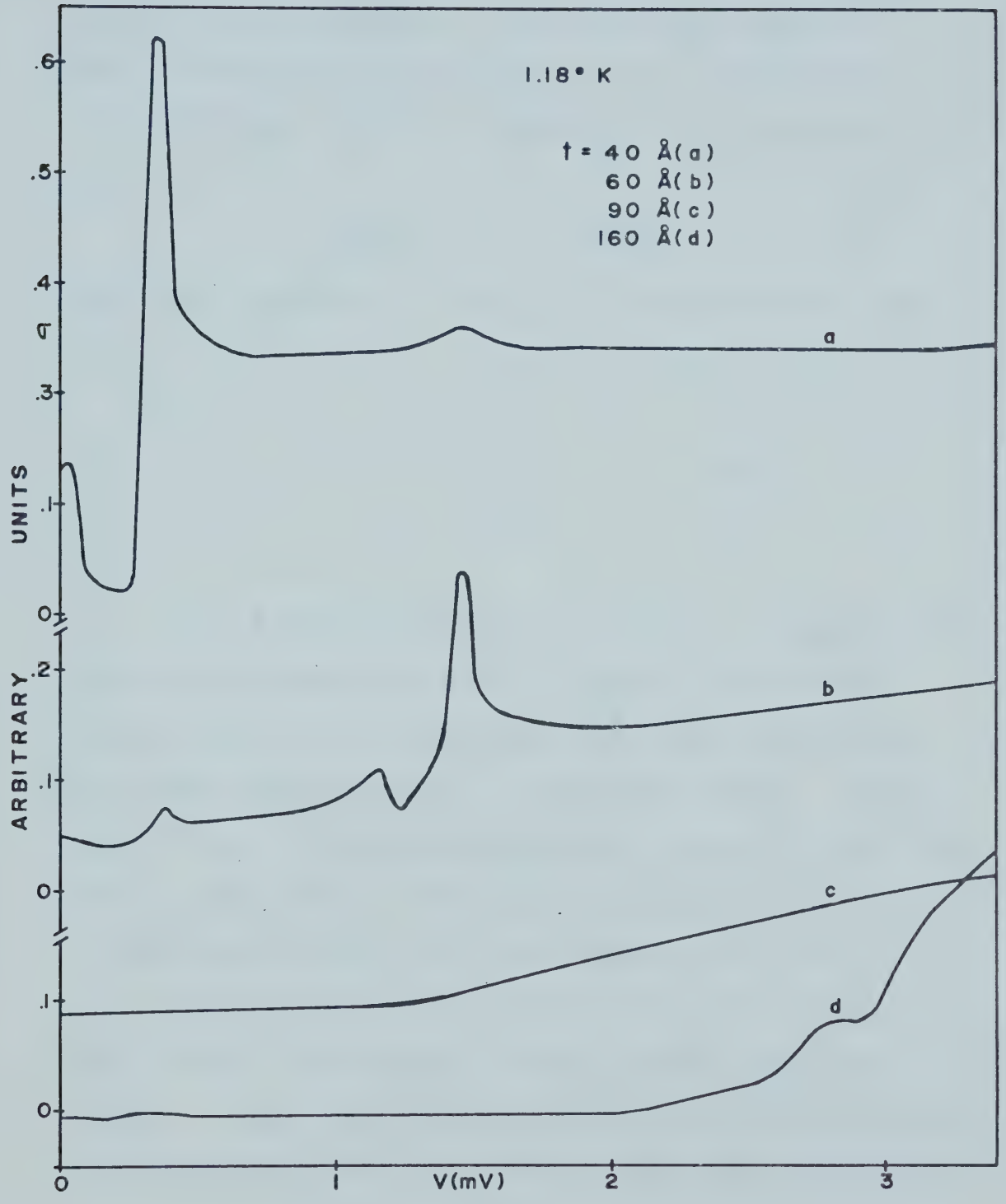

Figure 5.15. Conductance versus voltage of four different junctions of Al-Pb^{P}-Al at 1.18°K.

the particles. In curves (c) and (d) tunneling via particles is prominent. The second derivatives of such curves are shown in figure 5.16. In addition, one sees $2\Delta_{Pb}$. Table 5.1 summarises the results.

Table 5.1 (1.08°K)

Particle thickness Å	$2\Delta_{Pb}$ mV	Particle energy gap $(2\Delta_{Al} + 2\Delta_{Pb})$ mV
60	2.52	2.94
80	2.62	3.00
130	2.66	3.06

Some junctions had multiple peaks at temperatures when Al was superconducting. Figure (5.17a) shows conductance-voltage characteristic when Pb particles are normal characteristic of particle effect. When both Al and Pb are superconducting, figure (5.17b), two peaks appear at 0.27 mV and 0.41 mV instead of one at .35 mV, and another small peak appears at 1.4 mV. This is a result of some particles being in contact with Al film giving rise to what is known as the "proximity" effect. Vrba (1971) has observed such multiple peaks. De Gennes-Werthamer (1963) theory gives the properties of proximity sandwitches. When a superconductor is in contact with a normal metal, the normal may become

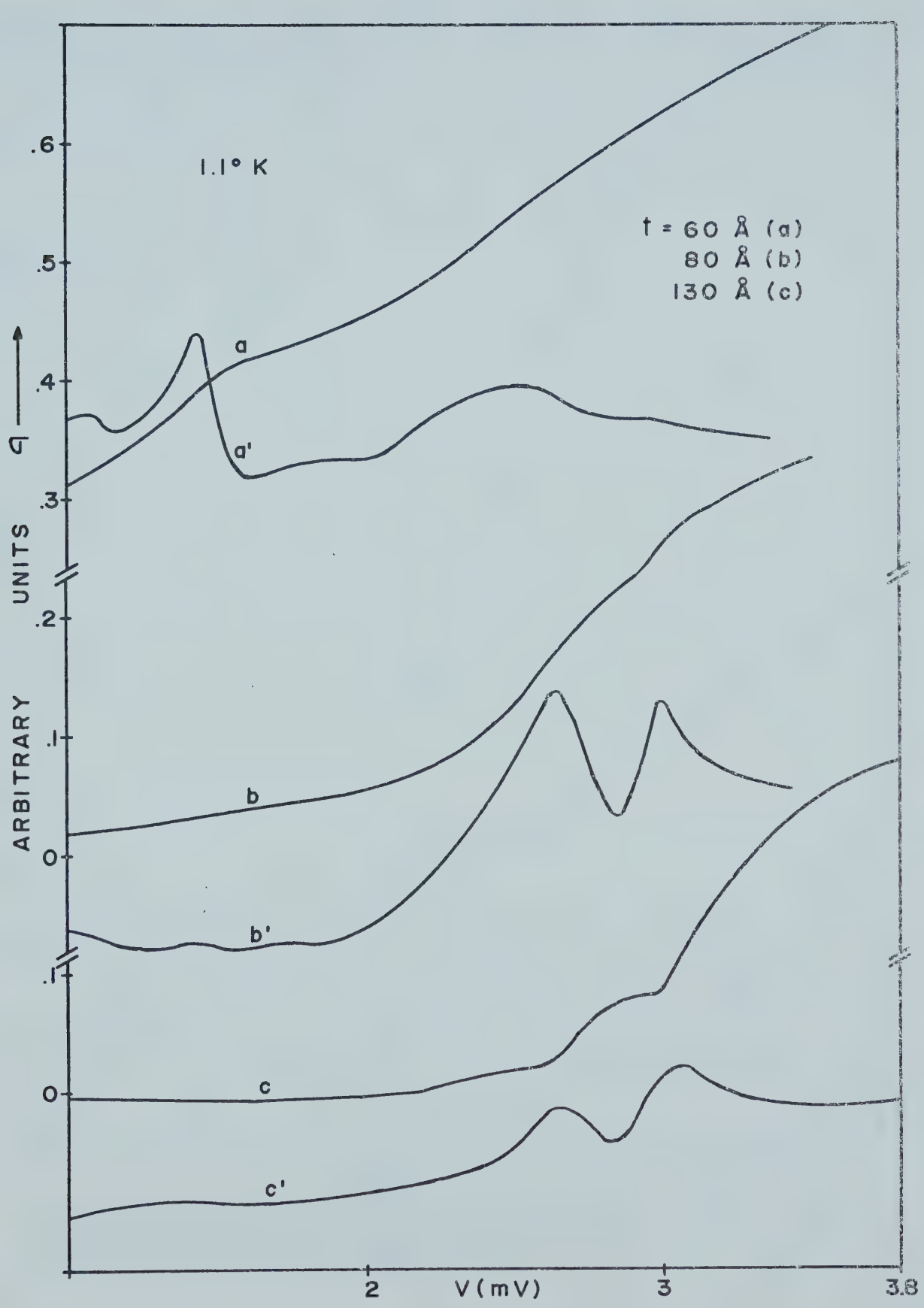

Figure 5.16. Second derivative of the conductance showing energy gaps for three different junctions.

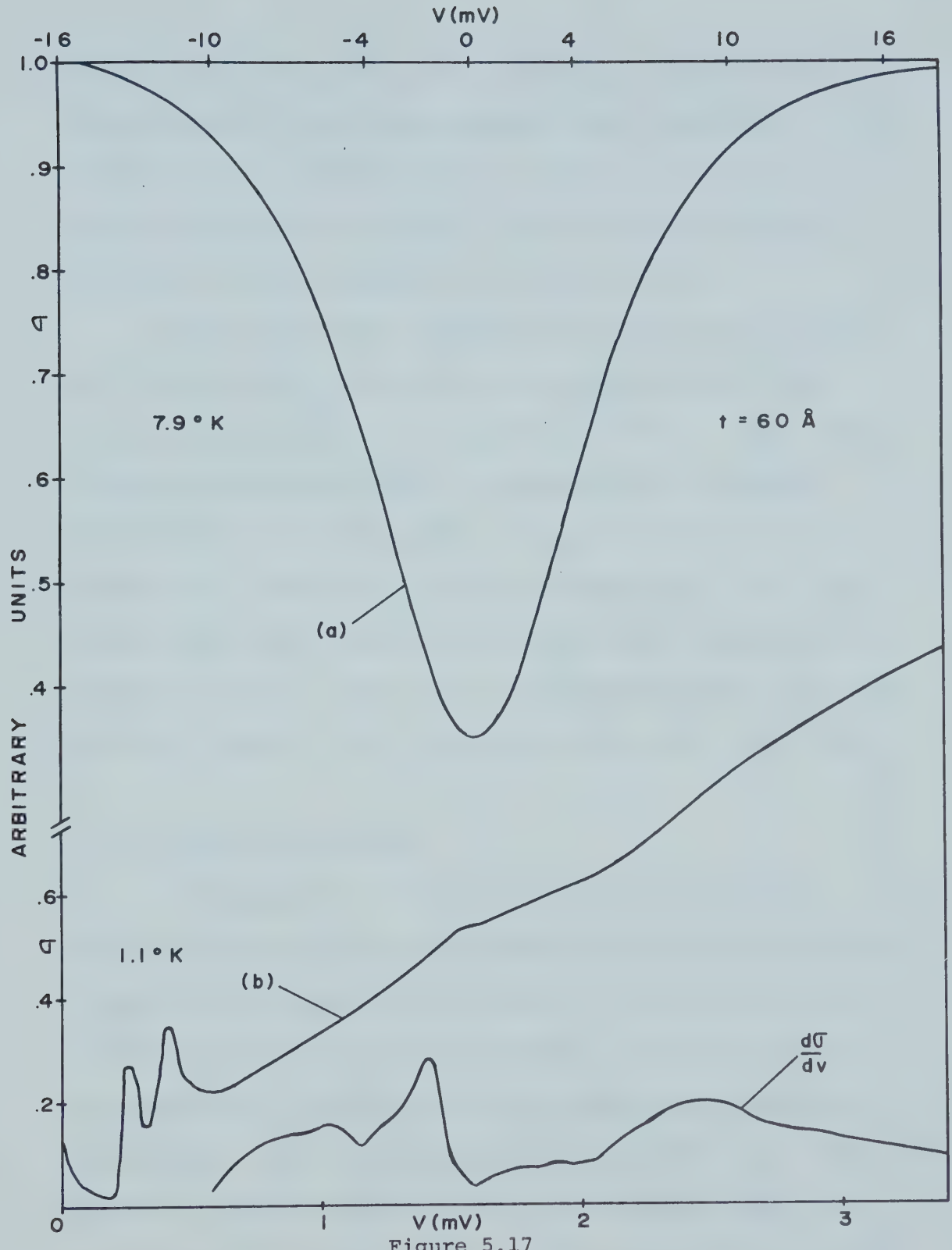

Figure 5.17

(a) Conductance versus voltage with Pb particles normal
(b) Multiple peaks of superconducting Al
(c) Second derivative of curve (b)

superconducting while the transition temperature and energy gap of the superconductor are lowered; if in contact with a superconductor their properties may change resulting in energy gap and transition temperature values somewhere between the two.

The temperature dependence of the conductance was found to be linear when the Pb particles were normal in agreement with equation (3.26). When they became superconducting the conductance decreased moving away from linearity. Figure 5.18 shows the normalized conductance versus temperature. For the three different junctions the critical temperature is found to be the same, $7.4 \pm .05°K$, compared to $7.2°K$ for the bulk sample. The average ratio $2\Delta/kT_c$ was 4.14.

(iii) Phonon Structure

In Chapter 2 it was mentioned that Fröhlich discussed the attraction between electrons as arising from electron-phonon interactions. Rowell and Kopf (1964) studied the phonon spectrum involved in the interaction. Solutions of the energy gap equation by Swihart (1963) and Culler at al (1962) show that phonon structure should occur at energies $\Delta+E_D$ and $\Delta+E_E$ where E_D is the Debye cut off energy at cut off frequency ω_c and E_E is the Einstein peak. Morel and

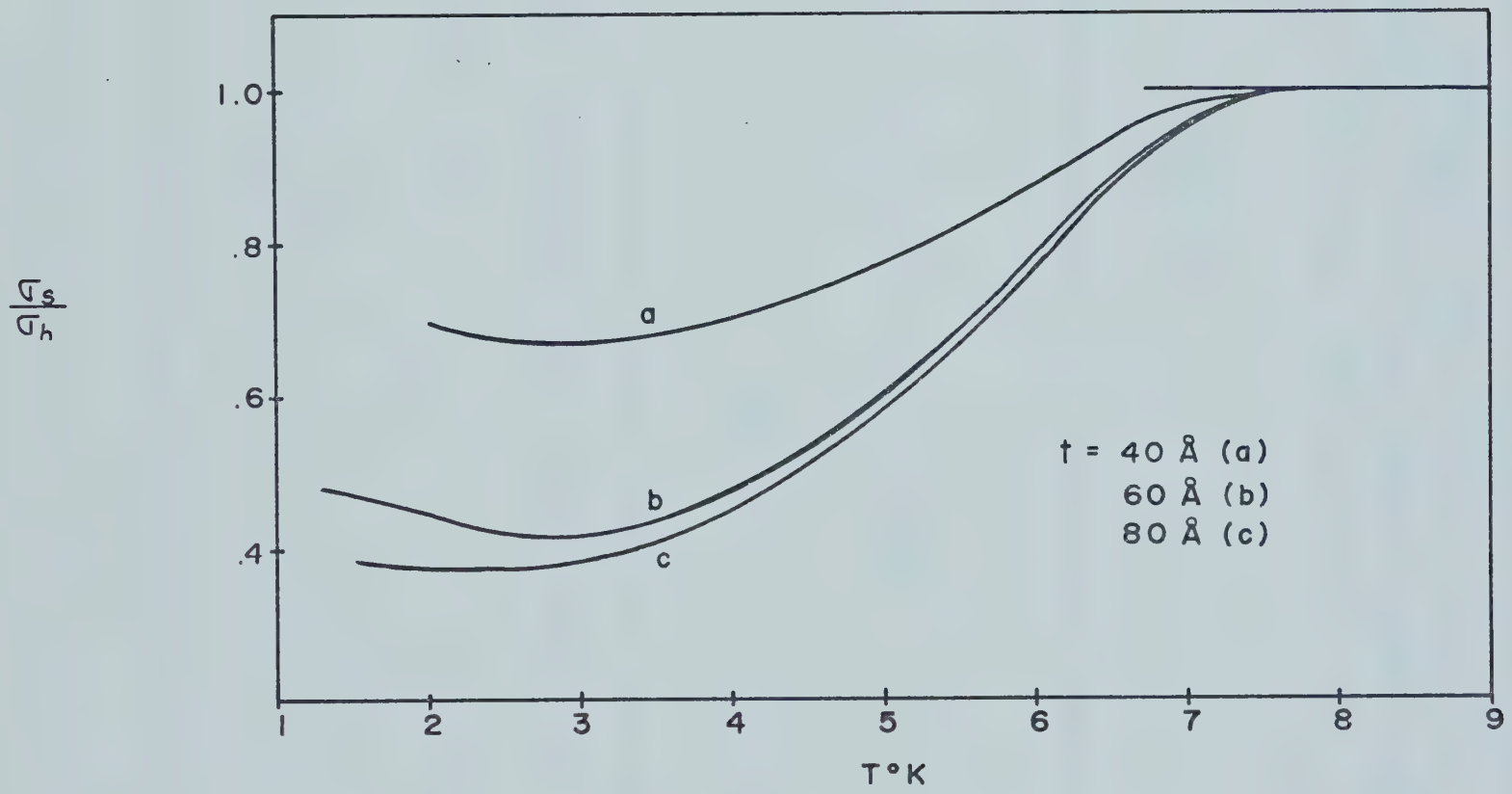

Figure 5.18. The normalized conductance versus temperature for three different junctions of Al-Pb^{P}-Al.

The background conductance for three junctions is found to be 24%, 15% and 7% for t = 40Å, 60Å and 80Å respectively.

Anderson carried on further calculations showing that for the Einstein peak, the density-of-states structures should be observed at $\Delta+E_E$, $\Delta+2E_E$, $\Delta+3E_E$, etc.

Adler et al (1963) have observed phonon structures of lead, tin and indium. From equation (3.17b)

$$\sigma = \mathrm{Re}\ \{\frac{V}{(V^2 - \Delta^2)^{\frac{1}{2}}}\} \quad .$$

In the BCS approximation $V >> \Delta$ and by the Taylor series expansion

$$\sigma_{BCS} = \frac{V}{(V^2 - \Delta^2)^{\frac{1}{2}}} = 1 + \frac{1}{2}\frac{\Delta^2}{V^2} + \frac{3}{4}(\frac{\Delta^2}{V^2})^2 + \ldots$$

$$\simeq 1 + \frac{\Delta^2}{2V^2} \quad . \qquad 5.4$$

But due to quasiparticle damping and life time effects one includes an imaginary part in the energy gap.

$$\Delta = \Delta_1 + i\Delta_2 \qquad 5.5$$

so that

$$\sigma \simeq 1 + \frac{\Delta_1^2 - \Delta_2^2}{2V^2} \quad . \qquad 5.6$$

Adler et al define the phonon strength factor $S(V,T)$ as

$$S(V,T) = \sigma_{BCS} - \sigma$$

$$\simeq \frac{1}{2V^2}\,(\Delta_o^2 - \Delta_1^2 + \Delta_2^2)$$

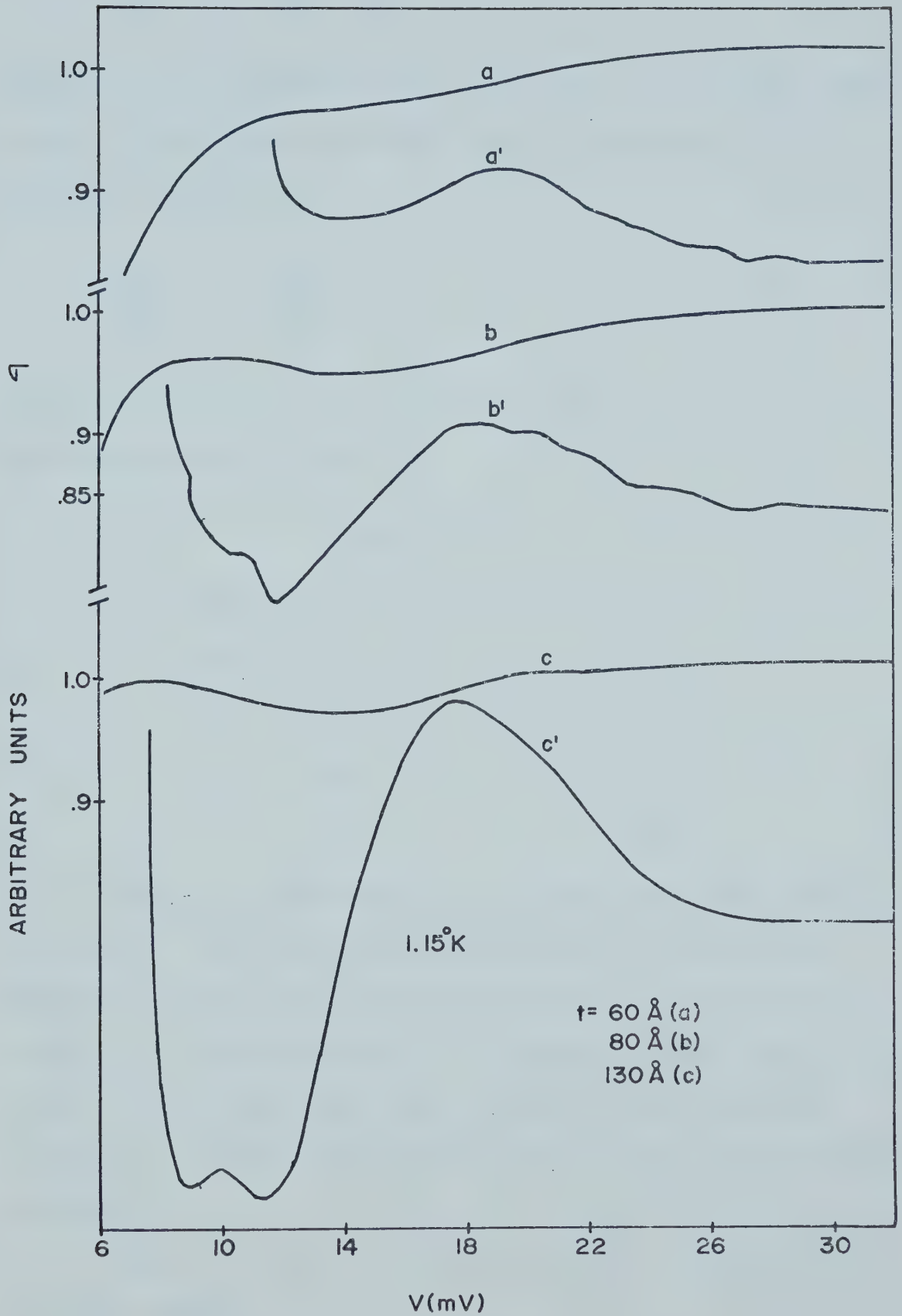

Figure 5.19. Phonon structure for three different junctions of Al-Pb^{P}-Al.

a', b' and c' are the second derivatives of a, b and c curves respectively.

$$\frac{2V^2_S}{\Delta^2_o} \simeq 1 - \frac{\Delta^2_1}{\Delta^2_o} + \frac{\Delta^2_2}{\Delta^2_o} \quad . \qquad 5.7$$

According to the Schrieffer, Scalapino and Wilkins (1963) model, Δ_1 becomes very small and Δ_2 increases at the phonon voltages V_p.

$$\frac{2V^2_S}{\Delta^2_o} \simeq 1 + \frac{\Delta^2_2}{\Delta^2_o} \quad . \qquad 5.8$$

Figure 5.19 shows the phonon structures and the results are summarised in table 5.

Table 5.2

Observed Phonon Structure Voltages

Particle size (Å)	V_p (mV)
60	13.8 ± .1
80	11.8 ± .1
130	8.8 ± .1

There is a broadening which smears out the singularities. This broadening is predicted by Dickey and Paskin (1968) in their calculations of phonon spectrum changes in small particles. V_p depends on the particle size. It is higher for small particles and decreases tending to the bulk value of 8.5 mV as the sizes particles increase.

Table 5.3 shows the particle results compared to the bulk values.

Table 5.3

Particle results compared to the bulk values

Material	Particle size, Å	T_c °K	$2\Delta_o$ (mV)	$\frac{2\Delta_o}{3.5kT_c}$	Background conductance %	Bulk Values			
						T_c °K	$2\Delta_o$ (mV)	$\frac{2\Delta_o}{3.5kT_c}$	Reference
Sn	65	4.15±.05	1.3 ±.05	3.63	27	3.85	1.22	3.67	Walmsley and Campbell (1967).
	90	4.5 ±.1	1.25±.05	3.22	4				
	130	4.05±.05	1.25±.1	3.68	14				
Pb	40	-	-	-	24	7.2	2.66	4.45	Zavarritskii (1961).
	60	7.4 ±.05	2.59±.01	4.07	15				
	80	7.4 ±.05	2.65±.01	4.14	7				
	130	7.4 ±.05	2.71±.01	4.25	-				

CHAPTER 6

CONCLUSION

The capacitor model has been used to explain results of tunneling via particles in the normal state. In the superconducting state tunneling via particles exhibits two junctions in series characteristics.

There is a particle size dependence of the critical temperature of tin particles. Bucket and Hisch (1952) found that the size dependence of the critical temperature of a thin film depends on the temperature at which the film was formed. All our junctions were prepared at room temperature. According to Bucket-Hisch observation, a higher percentage change in T_c would be obtained if the particles were deposited at a lower temperature. Due to the low magnetic field attainable, we could not keep the particles normal at low temperatures by applying a magnetic field.

The energy gap results do not conclusively show a particle size dependence of the energy gap. In the case of lead particles $2\Delta_{Pb}$ show a 2.2% variation about 2.65 mV. There is a big uncertainty in the ratio $2\Delta/kT_c$ since T_c could not be determined precisely.

The phonon structure in lead is so strong that it can be observed in superconducting lead particles.

REFERENCES

Adler, J.G. (1963), Electron Tunneling into Superconductors (Doctoral Thesis, University of Alberta).

Adler, J.G., Rogers, J.S. and Woods, S.B. (1965), Can. J. Phys. 43, 557.

Anderson, P.W. (1959), J. Phys. Chem. Solids 11, 26.

Bardeen, J. (1961), Phys. Rev. Letters 6, 57.

Bardeen, J., Cooper, L.N. and Schrieffer, J.R. (1957), Phys. Rev. 108, 1175.

Basset, C.A., Menter, J.W., Pashley, D.W. (1959), Structure and Properties of Thin Films (John Wiley and Sons, N.Y.).

Blumberg, R.H. and Seraphin, D.P. (1963), J. Appl. Phys. 33, 163.

Bucket, W. and Hisch, R. (1952), Z. Physik 131, 420.

Carbotte, J.P. and Dynes, R.C. (1968), Phys. Letters 25A, 685.

Carbotte, J.P. and Dynes, R.C. (1967), Phys. Rev. 172, 476.

Chakraverty, B.K. (1967) in Proceedings of Second Colloquium on Thin Films (Haln, E. Ed.).

Chopra, K.L. (1969), Thin Film Phenomena (McGraw-Hill, N.Y. (1969)).

Cohen, M.H., Falicov, L.M. and Phillips, J.C. (1962), Phys. Rev. Letters 8, 316.

Cooper, L.N. (1956), Phys. Rev. 104, 1189.

Cooper, L.N. (1959), Am. J. Phys. 28, 91.

Culler, G.J., Fried, B.O., Huff, R.W. and Schrieffer, J.R. (1962), Phys. Rev. Letters 8, 399.

Dickey, J.M. and Paskin, A. (1968), Phys. Rev. Letters 21, 1441.

Eschbach, H.L. and Kruidhof, W.E. (1965) in Vacuum Microbalance Tech. 3, 207.

Fisher, J.C. and Giaever, I. (1961), J. Appl. Phys. 32, 172.

Fröhlich, H. (1950), Phys. Rev. 79, 845.

Gennes, P.G., Superconductivity of Metals and Alloys, (Benjamin (1960)).

Giaever, I. (1960a), Phys. Rev. Letters 5, 147.

Giaever, I. (1960b), Phys. Rev. Letters 5, 464.

Giaever, I., Hart, H.R. and Megerle, K. (1962), Phys. Rev. 126, 941.

Giaever, I. and Megerle, K. (1962), Phys. Rev. 122, 1101.

Gilat, G. and Raubenheimer, J.L. (1966), Phys. Rev. 144, 390.

Ginzberg, V.L. and Landau, L.D. (1950), J.E.T.P. 20, 1064.

Gorter, C.J. and Casimir, H.B.G. (1934a), Physica 1, 306.

Gorter, C.J. and Casimir, H.B.G. (1934b), Phys. Z. 35, 963.

Handy, R.M. (1962), Phys. Rev. 126, 1968.

Hartman, T.E. (1965), J. Vacuum Tech. 3, 28.

Holland, L. (1963), Vacuum Deposition of Thin Films (Chapman and Hall, London (1963)).

Khukhareva, I.S. (1961), J.E.T.P. 41, 728.

Kupper, C.G. (1968), Introduction to the Theory of Superconductivity (Oxford (1968)).

London, F. (1936), Physica 3, 450.

London, F., Superfluids, Vol. I (New York, Wiley, 1950).

Lynton, E.A. (1962), Superconductivity (Chapman and Hall Ltd., London (1971)).

Markowitz, D. (1967), Phys. 3, 199.

Mathias, B. (1967), Prog. Low. Temp. Phys. 2, 13.

Maxwell, E. (1950), Phys. Rev. 78, 477.

Mezei, F. (1972), Phys. Rev. B 4, 3775.

Miles, J.L. and Smith, P.H. (1963), J. Elech. Soc. 110, 1240.

Morel, P. and Anderson, P.W. (1962), Phys. Rev. 125, 1263.

Neugebaur, C.A. and Webb, M.B. (1962), J. Appl. Phys. 33, 74.

Parmenter, R.H. (1968), Phys. Rev. 166, 392.

Pippard, A.B. (1953), Proc. Roy. Soc. 47, 617.

Pocza, J.F. (1967) in Proceedings of Second Colloquium of Thin Films (Haln E. Ed.).

Prange, R. (1963), Phys. Rev. 131, 1083.

Reuter, G.E.H. and Sondheimer, E.H. (1948), Proc. Roy. Soc. A195, 336.

Reynolds, C.A., Serin, B., Wright, W.H. and Nesbitt, L.B. (1950), Phys. Rev. 78, 487.

Rogers, J.S. (1964), Electron Tunneling into Superconductors (Doctoral Thesis, University of Alberta).

Rogers, J.S. (1970), Rev. Sci. Inst. 41, 1184.

Rowell, J.M. and Kopf, L. (1965), Phys. Rev. 137, A907.

Schrieffer, J.R. (1963), Theory of Superconductivity (Benjamin Publishers (1964)).

Schrieffer, J.R., Scalapino, D.J. and Wilkins, J.W. (1963), Phys. Rev. Letters 10, 336.

Schrieffer, J.R. (1963), Phys. Rev. Letters 10, 17.

Sevastyonov, B.K. (1961), J.E.T.P. 40, 52.

Swihart, J.C. (1963), Phys. Rev. 131, 72.

Tewordt, L. (1962), Phys. Rev. 128, 371.

Tewordt, L. (1962), Phys. Rev. 128, 12.

Tinkham, T. (1965), Superconductivity (Gordon and Breach Sci. Publishers, N.Y.).

Townsend, P., Gregory, S. and Taylor, R.G. (1972), Phys. Rev. B 5, 54.

Wallace, P.R. (1969), Superconductivity (Gordon and Breach Sci. Publishers, N.Y.).

Walmsley, D.G. (1965), Anisotropy Effects in Superconductive Tunneling (Doctoral Thesis, McMaster University).

Walmsley, D.G. and Campbell, C.K. (1967), Can. J. Phys. 45, 1541.

Warner, A.W. and Stockbridge, C.D. (1963), J. Appl. Phys. 34, 437.

Wethamer, N.R. (1963), Phys. Rev. 132, 2440.

Vrba, J. (1971), Tunneling into Weakly Coupled Films of Al and Sn Proximity (Doctoral Thesis, University of Alberta).

Zeller, H.R. and Giaever, I. (1968), Phys. Rev. 181, 789.